Quaternary Science Reviews 228 (2020) 106103

Contents lists available at ScienceDirect

Quaternary Science Reviews

journal homepage: www.elsevier.com/locate/quascirev

Highly branched isoprenoids reveal onset of deglaciation followed by dynamic sea-ice conditions in the western Amundsen Sea, Antarctica

Nele Lamping [a, *], Juliane Müller [a, b, c], Oliver Esper [a], Claus-Dieter Hillenbrand [d], James A. Smith [d], Gerhard Kuhn [a]

[a] Alfred-Wegener-Institut Helmholtz-Zentrum für Polar- und Meeresforschung, Am Alten Hafen 26, 27568, Bremerhaven, Germany
[b] Department of Geosciences, University of Bremen, Klagenfurter Straße, 28359, Bremen, Germany
[c] Marum - Center for Marine Environmental Sciences, Leobener Straße 8, 28359, Bremen, Germany
[d] British Antarctic Survey, High Cross, Madingley Road, Cambridge, CB3 0ET, United Kingdom

ARTICLE INFO

Article history:
Received 12 July 2019
Received in revised form
22 November 2019
Accepted 22 November 2019
Available online 9 December 2019

Keywords:
Quaternary
Palaeoclimatology
Antarctica
Marine biomarkers
HBIs
$IPSO_{25}$
Sea ice
West Antarctic Ice Sheet

ABSTRACT

The Amundsen Sea drainage sector of the West Antarctic Ice Sheet (WAIS) is widely regarded as a candidate for triggering potential WAIS collapse. The grounded ice sheet drains into the Amundsen Sea Embayment and is thereby buttressed by its fringing ice shelves, which have thinned at an alarming rate. Satellite-based observations additionally reveal a considerable long-term decrease in sea-ice cover in the Amundsen Sea over the last two decades although the long-term significance of this trend is unclear due to the short instrumental record since the 1970s. In this context, investigations of past sea-ice conditions are crucial for improving our understanding of the influence that sea-ice variability has on the adjacent marine environment as well as any role it plays in modulating ice shelf and ice sheet dynamics. In this study, we apply novel organic geochemical biomarker techniques to a marine sediment core from the western Amundsen Sea shelf in order to provide a valuable long-term perspective on sea-ice conditions and the retreat of the Getz Ice Shelf during the last deglaciation. We analysed a specific biomarker lipid called $IPSO_{25}$ alongside a phytoplankton biomarker and sedimentological parameters and additionally applied diatom transfer functions for reconstructing palaeo sea-ice coverage. This multi-proxy data set reveals a dynamic behaviour of the Getz Ice Shelf and sea-ice cover during the deglaciation following the last ice age, with potential linkages to inter-hemispheric seesaw climate patterns. We further apply and evaluate the recently proposed $PIPSO_{25}$ approach for semi-quantitative sea-ice reconstructions and discuss potential limitations.

1. Introduction

Southern Ocean sea-ice cover is one of the most variable features on Earth's surface with extreme seasonal and often considerable interannual changes. Consequently, it plays a key role in the global climate system by influencing major atmospheric and oceanic processes (Thomas, 2017). Satellite-based observations of Antarctic sea ice reveal a positive overall trend in sea-ice extent from 1979 to 2014 (Comiso et al., 2017; De Santis et al., 2017; Parkinson and Cavalieri, 2012). Parkinson (2019) recently reported a reversal of this trend and note a decrease in Antarctic sea-ice extent since 2014, reaching record lows in 2017 and 2018. The positive overall trend, which is still displayed by the 40-y record (Parkinson, 2019), however, shows huge interannual variabilities and also large opposing regional trends. These regions include the Bellingshausen and Amundsen Seas, where a sustained decline in annual sea-ice cover has been observed since the 1970s, and the Weddell and Ross Seas, where the area of annual sea-ice cover has increased during the same time interval (Comiso et al., 2017; Parkinson and Cavalieri, 2012; Stammerjohn et al., 2012). Consequently, reconstructing regional (palaeo) sea-ice conditions is also crucial for understanding and interpreting current climate evolution and for improving predictions of its future (De Santis et al., 2017; Shepherd et al., 2018). Furthermore, sea-ice seasonality and sea-ice cover are poorly resolved in current climate models (Rosenblum and Eisenman, 2017) and proxy-based sea-ice

* Corresponding author. Am Alten Hafen 26, 27568, Bremerhaven, Germany
E-mail addresses: nele.lamping@awi.de (N. Lamping), juliane.mueller@awi.de (J. Müller), oliver.esper@awi.de (O. Esper), hilc@bas.ac.uk (C.-D. Hillenbrand), jaas@bas.ac.uk (J.A. Smith), gerhard.kuhn@awi.de (G. Kuhn).

https://doi.org/10.1016/j.quascirev.2019.106103

reconstructions provide a tool with which to validate and improve these predictive models (Vaughan et al., 2013).

Sea ice triggers complex feedback mechanisms in the global climate system. It is a limiting factor for the gas, heat and moisture exchange between the ocean and atmosphere (Bopp et al., 2003; Thomas, 2017) and also affects primary productivity and the thermohaline circulation (Perrette et al., 2011; Smith and Nelson, 1986; Smith, 1987). The bright surface of sea ice is highly reflective (high albedo) inhibiting oceanic uptake of incoming solar radiation (Hall, 2004; Massom et al., 2001). During sea-ice formation, brines are released into the water column, building a barrier of denser waters that preclude incursions of relatively warm deep waters from entering sub-ice shelf cavities, consequently minimising basal melt of ice shelves in some regions (e.g. Hellmer et al., 2012). Brines also make a major contribution to the formation of Antarctic Bottom Water (AABW) (e.g. Nicholls et al., 2009). Furthermore, Massom et al. (2018) found that sea-ice presence in the vicinity of weakened or flooded ice shelves acts as a protective buffer by reducing the destructive effects of ocean swells.

In the Southern Ocean, proxy-based sea-ice reconstructions mainly rely on analyses of sea-ice associated diatom assemblages preserved in marine sediments to determine past positions of mean seasonal and perennial sea-ice extent and to infer relative shifts in the duration of the sea-ice/open water seasons (Allen et al., 2011; Crosta et al., 1998; Gersonde and Zielinski, 2000; Leventer et al., 1996; Leventer, 1998). Diatom-based transfer functions (TF) have allowed for quantitative reconstructions of sea-ice concentrations and sea surface temperatures (SSTs) (Armand et al., 2005; Benz et al., 2016; Crosta et al., 1998; Esper and Gersonde, 2014a; Gersonde et al., 2005; Zielinski et al., 1998), but the application of this TF approach can be limited due to dissolution effects of the thin silica frustules of diatoms within the water column or after deposition (e.g. Leventer, 1998; Zielinski et al., 1998). Highly branched isoprenoid (HBI) alkenes, organic geochemical lipids biosynthesized by certain diatoms have recently been shown to provide an alternative and robust proxy to reconstruct past Antarctic sea ice (Barbara et al., 2010; Collins et al., 2013; Denis et al., 2010; Etourneau et al., 2013; Massé et al., 2011). The di-unsaturated HBI alkene $C_{25:2}$ has been measured in Southern Ocean sediments and recently found to be produced by the Southern Ocean sympagic tube-dwelling diatom *Berkeleya adeliensis,* which is commonly associated with land-fast ice and consolidated platelet ice (Belt et al., 2016; Riaux-Gobin and Poulin, 2004). Because of its structurally close relationship to the well-established mono-unsaturated $C_{25:1}$ HBI, IP_{25}, in the Arctic Ocean (Belt et al., 2007; Belt and Müller, 2013; Belt, 2018), the term $IPSO_{25}$ (Ice Proxy for the Southern Ocean with 25 carbon atoms) was introduced (Belt et al., 2016). The Arctic sea-ice proxy IP_{25} was proven a reliable proxy for sea-ice conditions and has since been combined with open-water phytoplankton biomarkers, such as brassicasterol, dinosterol (Volkman, 1986; Volkman et al., 1993) or HBI trienes (HBI III; Smik et al., 2016), to obtain a more accurate picture of prevailing sea-ice conditions (Müller et al., 2009, 2011). The absence of $IPSO_{25}$ in the sediments can be the result of either permanent open-ocean conditions or a floating ice canopy (either a perennial sea-ice cover or ice-shelf cover), which prevents light penetration needed for ice algae growth. In order to avoid misinterpretations, the so called PIP_{25} index was established, with "P" representing an open-water phytoplankton biomarker (e.g. Belt and Müller, 2013; Müller et al., 2011; Xiao et al., 2015).

A common approach in Antarctic waters, so far, is the application of a ratio of $IPSO_{25}$ and an HBI triene ($C_{25:3}$), which may reflect the relative contributions of sea-ice and open-water phytoplankton inputs of organic matter, respectively, to the seabed sediments (Barbara et al., 2010; Collins et al., 2013; Denis et al., 2010; Massé et al., 2011). Recently, Vorrath et al. (2019) proposed a new approach for more semi-quantitative reconstructions of sea ice in Antarctica, following the PIP_{25} concept initially used in the Arctic. The so called $PIPSO_{25}$ index is, similar to PIP_{25}, a combination of the sea-ice proxy $IPSO_{25}$ and an open-water phytoplankton biomarker. The results obtained from surface sediments from the Antarctic Peninsula are in general agreement with sea-ice distribution data derived from satellite data and diatom assemblages, and suggest that the $PIPSO_{25}$ index may serve as a suitable approach for sea-ice reconstructions in Antarctica (Vorrath et al., 2019).

Reconstructions of palaeo sea-ice conditions in the Amundsen Sea are still sparse, yet knowledge about how the environment has changed is critical to better understand the current trend of declining sea ice (since the 1970s; Parkinson, 2019; Stammerjohn et al., 2015) in this climate sensitive area. Well-constrained proxy-records will lead to a more complete understanding of the long-term relationship between climate and sea-ice variability that will help to validate numerical model predictions of future scenarios of ice sheet dynamics and ocean-cryosphere interactions.

Here, we present the first biomarker-based palaeo-record for the western Amundsen Sea Embayment (ASE) shelf documenting the retreat of the Getz Ice Shelf and the onset of sea-ice coverage since the last deglaciation. The application of the sea-ice biomarker lipid $IPSO_{25}$ alongside the phytoplankton marker dinosterol enables us to reconstruct how the sea-ice/ice shelf cover in the western ASE has changed and how these changes might be linked to interhemispheric bipolar seesaw climate patterns. We compare our environmental interpretations based on the results of the organic geochemical biomarker analyses with interpretations derived from investigations of sedimentological proxies (Hillenbrand et al., 2010) and winter sea-ice (WSI) concentrations reconstructed from diatom TF on marine sediment core PS69/274-1.

2. Regional setting

North of the West Antarctic continental shelf of the Amundsen Sea, the Antarctic Circumpolar Current (ACC), the largest current system in the world (Meredith et al., 2011), flows in an eastward direction. Offshore from the ASE shelf, the Southern Boundary of the ACC (SBACC) marks the landward limit of the ACC and roughly divides the Seasonal Sea Ice Zone (affected by winter sea-ice cover) in the north from the perennial Sea Ice Zone in the south, where sea-ice cover persists throughout summer (Orsi et al., 1995). Waters on the continental shelf are characterised by the generally westward flowing Antarctic Slope Current (Mathiot et al., 2011) and are affected by seasonal (winter) and perennial sea-ice coverage (Fig. 1).

At present, perpendicular to the coast, relatively warm deep water, modified Circumpolar Deep Water (mCDW), is locally upwelling along deep glacially-carved troughs into the sub-ice shelf cavities of the continental shelf and up to the ice sheet grounding lines (e.g. Jacobs et al., 2011; Jenkins et al., 2010, 2018; Nakayama et al., 2013). The inflow of these relatively warm water masses is considered as a main driver for basal melting of ice shelves in the ASE (Hillenbrand et al., 2017; Jenkins et al., 2010, 2018; Shepherd et al., 2004; Thoma et al., 2008).

The inner shelf of the ASE is further characterised by the presence of two coastal polynyas, the Pine Island Polynya in Pine Island Bay and the Amundsen Sea Polynya (ASP) north of the Dotson and westernmost Getz ice shelves (Fig. 1; Alderkamp et al., 2012). Coastal polynyas play an important role in a number of physical and biological processes, such as sea-ice production, salt flux, water mass formation and elevated primary and secondary production, which is controlled by light availability at these high latitude environments (Arrigo and Van Dijken, 2003; Arrigo et al., 2015; Kern,

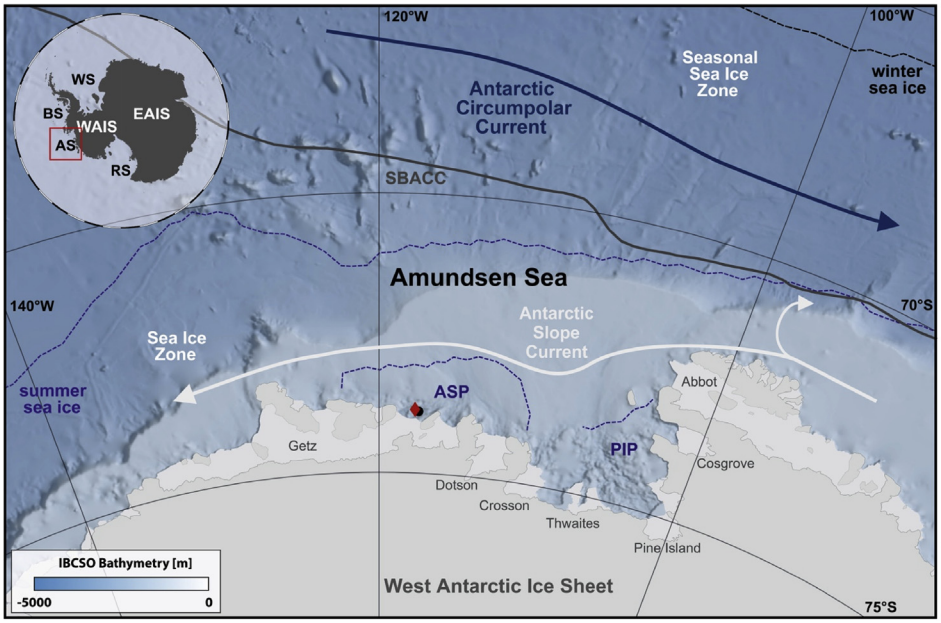

Fig. 1. Map of the Amundsen Sea (indicated by red box in insert map), showing the locations of marine sediment core PS69/274-1 (red diamond) and the nearby surface sediment sample from site PS69/275-2 (black dot). Summer sea-ice boundaries, polynyas and winter sea-ice boundaries are marked by dashed blue and black lines, respectively (Fetterer et al., 2016). Southern Boundary of the Antarctic Circumpolar Current (SBACC) is displayed as solid dark grey line and flow direction of the Antarctic Circumpolar Current (ACC) is indicated by the dark blue arrow. White arrows illustrate the flow direction of the Antarctic Slope Current (Mathiot et al., 2011; Orsi et al., 1995). Abbreviations: WAIS: West Antarctic Ice Sheet, EAIS: East Antarctic Ice Sheet, WS: Weddell Sea, BS: Bellingshausen Sea, AS: Amundsen Sea, RS: Ross Sea, ASP: Amundsen Sea Polynya, PIP: Pine Island Polynya. Background bathymetry derived from IBCSO data (Arndt et al., 2013). Insert map shows extent of grounded ice only (i.e., no ice shelves). (For interpretation of the references to color in this figure legend, the reader is referred to the Web version of this article.)

2009; Maqueda et al., 2004; Martin, 2001). The core analysed in this study is today located within the ASP (~27 000 km^2), which is the most biologically productive polynya in Antarctica (Arrigo and Van Dijken, 2003; Arrigo et al., 2012; Kim et al., 2015, 2016; Lee et al., 2017; Yager et al., 2012). In the ASP region, the length of the sea-ice season has declined by 60 ± 9 days since 1979, which is attributed to the earlier opening of the ASP in the year by 52 ± 9 days (Yager et al., 2012).

The mean seasonal sea-ice cover in the coastal area of the western ASE lasted on average 314 days per year during the period from 1979 to 2013, and annual sea-ice cover between 1993 and 2013 was on average two months shorter than between 1979 and 1992, associated with changes in spring sea-ice retreat (Stammerjohn et al., 2015). The trend in sea-ice area for the period from 1979 to 2014 in the Bellingshausen and Amundsen Seas was the only one that is negative around Antarctica, with an average decrease of −3.2% ± 1.4% decade^{-1} (Parkinson, 2019).

3. Material and methods

3.1. Material

Gravity core PS69/274-1 (73.85°S, 117.78°W; 1452 m water depth; recovery 4.51 m) and nearby giant box core PS69/275-2 (73.89°S, 117.55°W; 1472 m water depth), which provided an undisturbed seafloor surface sediment sample, were collected offshore from the westernmost Getz Ice Shelf on the western ASE shelf (Fig. 1) during RV *Polarstern* cruise ANT-XXIII/4 in 2006 (PS69; Gohl, 2007). Sediment core PS69/274-1 was previously divided into three lithological units by Hillenbrand et al. (2010). Unit I (0–196 cm) was described as bioturbated and stratified mud and silty clay, Unit II (196–239 cm) as bioturbated and stratified diatomaceous ooze and diatomaceous mud. Unit III was split into two subunits with Unit IIIa (239–317 cm) comprising bioturbated mud, sandy mud and muddy sand (with diatoms) and Unit IIIb (317–451 cm) comprising strongly laminated to stratified mud, sandy mud and muddy sand barren of diatoms. In this study, we adopt the age model of core PS69/274-1 (Table 1) obtained by radiocarbon dating of the acid-insoluble organic fraction (AIO) of the sediments and constrained by relative palaeomagnetic intensity (RPI) dating (Hillenbrand et al., 2010; Smith et al., 2011).

The oldest AIO ^{14}C age obtained from a sample at 311.5–312.5 cmbsf (24 543 cal. a BP) is considered unreliable because of significant contamination with reworked fossil organic carbon (Hillenbrand et al., 2010), which is supported by observations that the proximity of the grounding line during sediment deposition in a

Table 1
Age model for core PS69/274-1 based on radiocarbon dating of the acid insoluble organic fraction (AIO) and published by Hillenbrand et al. (2010). Conventional ^{14}C ages, local contamination offset (LCO) and calibrated ^{14}C ages are given. For the calibration, the LCO corrected age and the Southern Ocean marine reservoir effect of 1 300 ± 100 years (ΔR = 900 ± 100 years) (e.g., Berkman and Forman, 1996) were used. Unreliable ages are highlighted in italics.

Sample depth [cmbsf]	Lithology	Lithological unit	Conventional ^{14}C age [^{14}C a BP]	LCO [a]	LCO corr. age [corr.^{14}C a BP]	Age model [cal. a BP]
59.5–60.5	Mud	D	7 740 ± 39	2 650	5 090	4 272
139.5–140.5	Mud	D	14 199 ± 61	2 650	11 549	11 968
231.5–232.5	Diatomaceous ooze	C	11 967 ± 49	0	11 967	12 681
311.5–312.5	*Mud*	*B*	*24 416 ± 198*	*2 650*	*21 766*	*24 534*

proglacial setting leads to high inputs of reworked fossil carbon (Domack, 1992; Heroy and Anderson, 2007). Due to the relative coarse resolution of the age model, the proxies are plotted versus depth and the age model is presented as age constraints on the depth-axis. However, data presented along an age-axis are presented in Supplementary Figs. 1 and 22.

3.2. Bulk sediment and biomarker analyses

The sediment samples (avg. of ca 13 g) were stored in glass vials at −20 °C before and after being freeze-dried and homogenized with a mortar. Prior to the grinding, the coarse fraction comprising coarse sand and gravel (>0.5 mm) was removed from the sediment by sieving and converted into weight percent. After the removal of inorganic carbon (carbonates, total inorganic carbon) with 500 μl 12 N hydrochloric acid, the analysis of total organic carbon (TOC) contents was conducted on 0.1 g of sediment and measured with a carbon-sulphur determinator (CS 2000; Eltra). Standards were measured for calibration before the sample analyses and after every tenth sample to ensure accuracy (error ± 0.02%). The weight percentages (wt%) of total carbon (TC) and nitrogen (TN) were analysed using a CNS (Elementar Vario EL III) analyser. The percentage of carbonate was calculated from the difference between the amount of TC and organic carbon, using the following equation: $CaCO_3$ (%) = (TC−TOC) × 8.333. The precision (relative standard deviation, 1σ) of the measurements was better than 4% and accuracy better than 1% relative. For biomarker analyses, ca 4 g of the freeze-dried and homogenized sediment was extracted using ultrasonication (3 × 15 min) and dichloromethane:methanol (3 × 6 ml; 2:1 v/v) as solvent. Prior to extraction, the internal standards 7-hexylnonadecane (7-HND; 20 μl/sample) and 5α-androstan-3-ol (40 μl for surface sample PS69/275-2, 60 μl for PS69/274-1) were added for later quantification of HBIs and sterols, respectively. Fractionation of the extract was achieved by open-column chromatography, using SiO_2 as stationary phase. Elution of the HBIs and sterols was conducted with 5 ml *n*-hexane and 8 ml ethylacetate:*n*-hexane (20:80 v/v), respectively. Sterols were silylated with 300 μl bis-trimethylsilyl-trifluoroacetamide (BSTFA; 60 °C; 2 h). Compound identification was carried out using a gas chromatograph (GC; Agilent Technologies 7890B fitted with a 30 m DB 1MS column, 0.25 mm diameter and 0.25 μm film thickness) coupled to a mass selective detector (MSD, Agilent Technologies 5977B, with 70 eV constant ionization potential, ion source temperature of 230 °C). For hydrocarbon analysis, the temperature program of the GC was set to: 60 °C (3 min), 150 °C (rate: 15 °C/min), 320 °C (rate: 10 °C/min), 320 °C (15 min isothermal) and for sterol analysis: 60 °C (2 min), 150 °C (rate: 15 °C/min), 320 °C (rate: 3 °C/min), 320 °C (20 min isothermal). Helium served as carrier gas. HBI and sterol compounds were identified based on their GC retention times and mass spectral characteristics (Belt et al., 2000; Belt, 2018; Boon et al., 1979). Quantification of each lipid was achieved by setting the integrated GC-MS peak area in relation to that of the respective internal standard and by normalizing the resulting ratios by means of an instrumental response factor obtained for the individual lipid (Belt et al., 2014; Fahl and Stein, 2012). For $IPSO_{25}$ quantification, the molecular ion (m/z 348) was used in relation to the fragment ion m/z 266 of the internal standard 7-HND (Belt, 2018). For sterol quantification, the molecular ion m/z 500 for dinosterol (4,23,24 trimethyl-5α-cholest-22 *E*-en-3β-ol) was compared to the fragment ion m/z 348 of the internal standard 5α-androstan-3-ol. The masses of $IPSO_{25}$ and dinosterol derived by the GC-MS were then converted to sedimentary concentrations using the mass of extracted sediment. Concentrations of $IPSO_{25}$ and dinosterol were corrected to the TOC contents of each sample.

Following Müller et al. (2011), we specified the $PIPSO_{25}$ index by using the subscript "D" as P_DIPSO_{25} which refers to the use of dinosterol as phytoplankton biomarker. The P_DIPSO_{25} index was calculated based on the following equation:

$$P_DIPSO_{25} = IPSO_{25}/(IPSO_{25} + (\text{dinosterol x } c)) \quad (1)$$

with *c* being a concentration balance factor to account for significant concentration differences between $IPSO_{25}$ and dinosterol calculated as the ratio of mean $IPSO_{25}$ concentration to mean dinosterol concentration (Müller et al., 2011). Means and standard deviations of $IPSO_{25}$, P_DIPSO_{25}, dinosterol and TOC for each unit and subunit can be found in Supplementary Table 1.

3.3. Diatom transfer function derived winter sea-ice concentrations

We reconstructed WSI concentrations with a TF developed by Esper and Gersonde (2014a), applying the Modern Analog Technique (MAT) (after Hutson, 1980). Statistical details, background of the method and its performance at different application levels in comparison with other estimation methods are presented in Esper and Gersonde (2014a). For this purpose, quantitative diatom slides were prepared following the standard techniques (Gersonde and Zielinski, 2000). For diatom counting, the methods of Schrader and Gersonde (1978) were applied using a Zeiss Axioplan 2 microscope at 1000x magnification. Diatoms were identified to species or species group level and, if possible, to forma or variety level. The taxonomy follows primarily Hasle and Syvertsen (1996), Zielinski and Gersonde (1997), and Armand and Zielinski (2001). Species and species groups used for sea-ice reconstructions exhibit close relationships to environmental variables (Zielinski and Gersonde, 1997; Armand et al., 2005; Crosta et al., 2005; Romero et al., 2005; Esper et al., 2010; Esper and Gersonde, 2014a, b). For estimating WSI concentrations we applied the TF MAT-D274/28/6an, comprising 274 reference samples from surface sediments in the western Indian, the Atlantic and the Pacific sectors of the Southern Ocean, with 28 diatom taxa and taxa groups, and an average of 6 analogs (Esper and Gersonde, 2014a). The WSI estimates refer to September sea-ice concentrations averaged over a time period from 1981 to 2010 at each surface sediment site (National Oceanic and Atmospheric Administration, NOAA; Reynolds et al., 2002, 2007). The reference data set is suitable for our approach as it uses a 1 deg. by 1 deg. grid, giving a higher resolution than previously used and results in root mean square errors of prediction (RMSEP) of 5.52% (Esper and Gersonde, 2014a).

4. Results and discussion

4.1. Reconstruction of the palaeoenvironment from proxies

Based on our organic geochemical records, content of coarse-grained terrigenous debris >0.5 mm (supplied either by icebergs or sea ice, or transported at the base of an ice shelf and at some distance from the grounding line), on the basis of C/N ratios, carbonate ($CaCO_3$) as well as TOC content and TF (diatom) results in addition to previously published magnetic susceptibility, shear strength, biogenic opal, smectite/chlorite ratios (Sm/Chl ratios) in the clay fraction and grain size data (Hillenbrand et al., 2010; Smith et al., 2011), the sediments of core PS69/274-1 can be divided into four units (A-D), reflecting the palaeoenvironmental changes in the western ASE since the last deglaciation (Figs. 2–4). These units do not correspond directly to the three main lithostratigraphic units defined by Hillenbrand et al. (2010) or the two facies units distinguished by Smith et al. (2011) because the biomarker data permit a more detailed reconstruction of the palaeo-sea surface conditions

and, for example, the identification of the first retreat of the floating ice canopy from the core site and the onset of favourable growth conditions for biomarker synthesizing phytoplankton and sea-ice diatoms. The biomarker data are the main basis for the new definition of these units, which are now numbered chronologically from A to D (with Unit A being the oldest and Unit D being the youngest), which are then discussed and compared with the already published data by Hillenbrand et al. (2010) for reconstructing the palaeoenvironmental changes in the western ASE (Fig. 3).

4.1.1. Unit A: Floating ice canopy subsequent to grounding line retreat

In the lowermost unit of the core (Unit A; 451 to 317 cm below seafloor [cmbsf]), concentrations of the sea-ice biomarker lipid $IPSO_{25}$ and of the phytoplankton-derived biomarker dinosterol are below the detection limit (Fig. 2c and b, respectively). Hence, the calculation of the P_DIPSO_{25} index is not possible. The absence of both biomarker proxies suggests that the environmental conditions were not favourable either for open-water phytoplankton nor for $IPSO_{25}$ producing sea-ice diatoms. In previous studies, the absence of sea ice and phytoplankton-derived biomarkers in marine sediments has been interpreted to relate to a very thick ice cover (Belt, 2018; Müller et al., 2009).

Such an ice cover would also explain the lack of diatom frustules in the corresponding sediments, which, together with the lack of bioturbation, was also attributed to ice-shelf or permanent sea-ice cover by Hillenbrand et al. (2010) (Fig. 3). Assuming that the core site was covered by a floating ice canopy during deposition of this unit we assigned a maximum P_DIPSO_{25} value of 1 to these samples to maintain the sea-ice scaling of the P_DIPSO_{25} results and aid visualisation (displayed as triangles in Figs. 2 and 3).

TOC and biogenic opal contents in Unit A are extremely low, varying around 0.1 wt% and 1 wt%, respectively (Figs. 2d and 3c), with the low opal content either reflecting the rare presence of fragments of siliceous microfossils (i.e., too tiny for being identified under a microscope) or being an artefact caused by the partial leaching of clay minerals or volcanic glass (e.g. Müller and Schneider, 1993). These low TOC and opal values thus indicate a time interval of low or absent biological production. The unit is characterised by the highest magnetic susceptibility values measured on the core, varying between 300 and 500 $\times$ 10^{-5} SI units (Fig. 3f), which points to a high input of terrigenous detritus from a nearby grounding line (see Hillenbrand et al., 2010; Smith et al., 2011). Clay mineral data from neighbouring gravity core PS69/275-1 (for site location, see Fig. 1), reveal high chlorite contents in sediments deposited as subglacial till or proximal to the grounding line (Ehrmann et al., 2011). Therefore, the relatively low Sm/Chl ratio around 0.6 in Unit A sediments of core PS69/274-1 (Fig. 3d; Smith et al., 2011) probably indicates sediment deposition not far away from the grounding line.

The grain size composition of Unit A is mainly dominated by mud (ca 80 wt%), but shows two distinct maxima in gravel and sand contents (<60 wt%) at 400 and 320 cmbsf (Smith et al., 2011), with coarse-grained debris >0.5 mm peaking at the same depths (<1.8 wt%; Fig. 3h and g). Such maxima in gravel and sand contents can be interpreted as the result of two episodes, when either freely drifting icebergs transported ice-rafted debris (IRD) to the core location or when the core site was located closer to the grounding line and affected by rain-out of debris from the base of an ice shelf. Hillenbrand et al. (2010) observed lamination and stratification in the corresponding core interval but also reported absence of diatoms. Based on the findings from the productivity proxies (TOC, biogenic opal and dinosterol contents), we conclude that Unit A was deposited under a floating ice canopy formed either by perennial sea-ice cover or part of the Getz Ice Shelf (Fig. 4; Unit A). The coarse-grained debris peaks together with the clay mineral data indicate a position of the core site not far away from the grounding line, suggesting that the site was most likely covered by an ice shelf. According to the oldest reliable AIO ^{14}C age from 232 cmbsf depth, Unit A must have been deposited earlier than 12.7 cal. ka BP, with the RPI age model for core PS69/274-1 constraining its deposition to the time before 13 ka (Table 1; Hillenbrand et al., 2010). We therefore conclude that the deposition of Unit A took place during the last deglaciation, subsequent to grounded ice-retreat (Smith et al., 2011). Grounded ice-retreat from the inner Antarctic continental shelf during that time has also been reported for other areas. For example, a reconstruction by Milliken et al. (2009) reveals initial decoupling of the ice sheet from Maxwell Bay (South Shetland Island) at ca 14 cal. ka BP, whilst a study by Sjunneskog and Taylor (2002) on a diatom abundance record from Palmer Deep (inner shelf west of the Antarctic Peninsula) indicates that grounded ice-retreat there occurred at ca 13.2 ka BP. Minzoni et al. (2017) report grounding line retreat from Ferrero Bay (inner shelf of the eastern ASE) before ~11 cal. ka, which coincides with WAIS retreat from inner Pine Island Bay (Hillenbrand et al., 2013). Given the deposition of Unit A, under a floating ice canopy, not far away from the grounding line, we assume that it was deposited at very high sedimentation rates, which are expected to be at least an order of magnitude higher than at more distal locations (Andrews, 1987; Domack and Mcclennen, 1996). Interestingly, Milliken et al. (2009) report extremely low sedimentation rates in a similar setting with sedimentation under a permanent floating ice canopy in Maxwell Bay, which highlights the need to consider geomorphological features and the relative distance to the grounding line of an ice shelf.

4.1.2. Unit B: Dynamic ice front

In Unit B, from 317 to 239 cmbsf, concentrations of the sea-ice biomarker lipid $IPSO_{25}$ range from 4 to 8 μg*g OC^{-1} and are significantly higher than in the underlying Unit A, except for an interval around 275 cmbsf, where the lipid is absent (Fig. 2c). Concentrations of the phytoplankton-derived biomarker dinosterol show a similar pattern; increased values of 200–400 μg*g OC^{-1} (Fig. 2b) relative to Unit A, interrupted by its absence at ca 275 cmbsf. The P_DIPSO_{25} index varies between 0.4 and 0.8 (Fig. 2a).

The overall higher concentrations of both biomarker proxies in sediments from Unit B, when compared to those in sediments of Unit A, suggest more favourable environmental conditions for phytoplankton and $IPSO_{25}$ producing sea-ice diatoms, which we interpret as a result of break-up or retreat of the Getz Ice Shelf and establishment of seasonally open marine conditions (Fig. 4; Unit B). Ice shelf break-up conditions would also explain the low but significant diatom frustule concentrations in Unit B (cf. Hillenbrand et al., 2010). This conclusion is supported by our diatom TF which indicates a WSI concentration of ca 90% during the deposition of this unit (Fig. 3a).

Also, TOC, $CaCO_3$ and biogenic opal contents in Unit B sediments range from 0.2 to 0.4 wt%, 1–3 wt% and 2 wt%, respectively, and thus are higher than in the underlying sediments (Figs. 2 and 3), indicating increased marine productivity. The magnetic susceptibility generally decreases upwards throughout the unit to 200–350 $\times$ 10^{-5} SI units, suggesting a reduction in the supply of terrigenous detritus or increase in supply of biogenic material. A peak of 350 $\times$ 10^{-5} SI units at ca 275 cmbsf interrupts the decreasing trend, pointing to a higher terrigenous input as it is evident from a coinciding distinct maximum in coarse-grained debris >0.5 mm (1.7 wt%; Fig. 3). The grain-size is dominated by mud (>90 wt%) throughout Unit B (Fig. 3h), pointing to a grounding line distal glacimarine depositional setting (Hillenbrand et al., 2010; Smith et al., 2011). According to the RPI age model, Unit B

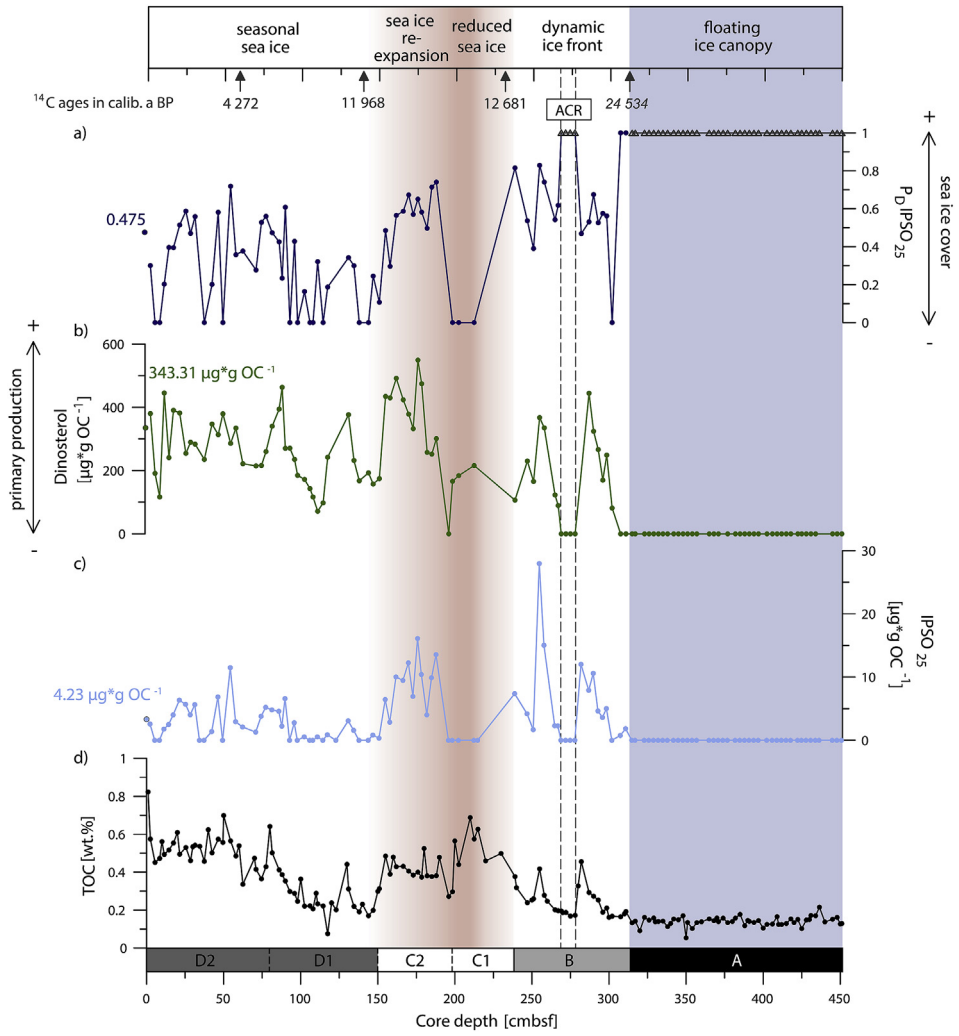

Fig. 2. Contents of P_DIPSO_{25} (a), dinosterol (b), $IPSO_{25}$ (c) and TOC (d) in sediment core PS69/274-1. AMS ^{14}C age constraints in calib. a before present (BP) in dark grey; unreliable age given in italics (Hillenbrand et al., 2010). Interval highlighted by dashed grey line marks the Antarctic Cold Reversal (ACR; Jouzel et al., 1995). Biomarker concentrations and calculated P_DIPSO_{25} value of the surface sample (box core PS69/275-2) indicated by dots with black circle and label in respective color. Triangles in P_DIPSO_{25}-curve: thick ice cover, maximum value of 1 assigned to these samples. Core is divided into four units as indicated in the lowermost and topmost bar: Unit A: floating ice canopy (blue shading), Unit B: dynamic ice front, Unit C: reduced sea ice/sea-ice re-expansion (red shading), Unit D: seasonal sea ice. (For interpretation of the references to color in this figure legend, the reader is referred to the Web version of this article.)

is older than 12.7 cal. ka. Importantly, our new biomarker record provides greater detail than previous sedimentological studies (Hillenbrand et al., 2010; Smith et al., 2011), by revealing the onset of seasonal open-marine productivity at 317 cmbsf. This is shown by the rapid increase of both biomarkers from 317 to ca 280 cmbsf and intermediate to high P_DIPSO_{25} values. Based on a new study on marine sediments from the Antarctic Peninsula (Vorrath et al., 2019), such changes can result from a transition from extensive sea-ice cover to marginal sea-ice/ice-edge conditions. A similar transition from a floating ice canopy to sea-ice dominated conditions from ca. 14.1–14.8 ka to 10.1 ka BP has also been reported by Milliken et al. (2009) for Maxwell Bay.

We attribute the lack of both biomarkers from 278 to 269 cmbsf and the peak in magnetic susceptibility in this depth interval to a thick ice coverage, probably caused by an ice-shelf re-advance or the predominance of a perennial sea-ice cover and consequently also assign a maximum P_DIPSO_{25} value of 1 to these samples (displayed as triangles in Figs. 2 and 3). As Milliken et al. (2009) do not report (or resolve) such a specific cooling interval in Maxwell Bay, we note that this suggested re-advance in ice-cover at our relatively more ice-shelf proximal core site may result from changes in local oceanic and/or atmospheric circulation patterns or a rapid ice-shelf surge. However, taking account of the coarse resolution of the age model of core PS69/274-1, we contemplate that this hypothesised re-advance of the Getz Ice Shelf or development of perennial sea-ice cover tentatively may have been associated with the atmospheric cooling during the Antarctic Cold Reversal (ACR), which interrupted warming in Antarctica during the last deglaciation and lasted from 14.5 to 12.9 ka BP (Blunier et al., 1997; Blunier and Brook, 2001; Jouzel et al., 1995; WAIS Divide Project Members, 2013). The ACR coincided with the abrupt warming of the Bølling-Allerød interstadial in the North Atlantic and was characterised by Southern Ocean cooling and Antarctic sea ice reversing its deglacial retreat trend because of interhemispheric coupling mechanisms (Skinner et al., 2010). These opposing climate trends of the two hemispheres are proposed to be driven by oceanic and/or atmospheric processes and referred to as the bipolar seesaw (Anderson et al., 2009; Broecker, 1998; Pedro et al., 2011). Hitherto, the temporal and spatial extent of the ACR is mainly documented in Antarctic ice cores (e.g. Pedro et al., 2016), while only few marine

records document re-advances of (sub-) Antarctic glaciers and elevated WSI concentrations during this time period (Bianchi and Gersonde, 2004; Graham et al., 2017; Xiao et al., 2016). Xiao et al. (2016), for example, compiled high resolution diatom composition records from the Antarctic Zone of Atlantic and Western Indian sectors of the Southern Ocean and determined the variability in summer sea surface temperatures and sea-ice conditions of the past 30 ka. They report a cooling observed in all investigated cores at 14-12 ka. Graham et al. (2017) used sea-floor geophysical data and marine sediment records off South Georgia and conclude on a cooling between 15.2 and 13.3 ka, both linking these cooling events to the ACR, revealing that this climate pattern extended up into the Atlantic sector of the Southern Ocean. Hence, locations more distal to the ice sheet (such as Southern Ocean pelagic records) seem to reflect atmospheric climate patterns rather than local trends, whilst locations in closer proximity to the ice shelf (such as our record), are much more likely influenced by, for example, a local or rapid ice-shelf surge.

Interestingly, in the sediments at ca 280 cmbsf, directly underlying the horizon of absence of both biomarkers, we observe a higher concentration of dinosterol as well as relative maxima in the TOC and $CaCO_3$ contents and in the Sm/Chl ratios (Fig. 3e and d). These peaks can be attributed to a short but significant warming period characterised by more open water conditions and higher productivity. Antarctic ice cores, such as the WAIS Divide Ice Core, and marine records from the Scotia Sea and the eastern Atlantic sector of the Southern Ocean (Xiao et al., 2016), also revealed a significant warming prior to the ACR during the Antarctic Isotope Maximum (AIM) 1 (Cuffey et al., 2016; WAIS Divide Project Members, 2013), which could have caused an increase in primary productivity reflected in higher dinosterol, TOC and $CaCO_3$ contents and of Sm/Chl ratios observed in core PS69/274-1 just shortly before the onset of the ACR. These elevated productivity proxies during AIM 1 argue against a perennial sea-ice or ice-shelf cover at the core site, though seasonal (winter/spring) sea ice must have occurred as it is indicated by the presence of $IPSO_{25}$ and diatom TF derived WSI concentrations of ca 90%.

4.1.3. Unit C: Reduced sea-ice cover followed by sea-ice re-expansion

Unit C in core PS69/274-1 (239-150 cmbsf) can be divided into two subunits (C1 and C2). Subunit C1 (239-196 cmbsf) comprises a diatomaceous ooze consisting of very well-preserved frustules of *Corethron pennatum*, which are considered open-water diatoms indicative of ice-free conditions (Maddison et al., 2005) and provided two AIO ^{14}C ages of 12.7 cal. ka BP, consistent with the RPI age constraints (Hillenbrand et al., 2010). The lower half of the subunit is not resolved by the biomarker data, while the upper half is characterised by the absence of the sea-ice biomarker $IPSO_{25}$ (Fig. 2c). Concentrations of the phytoplankton-derived biomarker dinosterol vary slightly around a value of 180 $\mu g^{*}g\ OC^{-1}$, also not resolving the lower half of the subunit (Fig. 2b). The calculated sea-ice index P_DIPSO_{25} is 0, indicating the absence of spring sea-ice cover and predominantly open water conditions during spring and summer (Fig. 2a; Belt, 2018; Müller et al., 2011). The relatively low dinosterol concentrations could be explained by unfavourable preservation conditions for organic compounds in the diatomaceous ooze, where an aggregation between fine-grained detritus and organic matter is severely restricted by the absence of silt and clay particles. Alternatively, either a limited nutrient supply in the open ocean could have reduced the productivity of dinosterol synthesizing phytoplankton species or exceptionally high sedimentation rates could have led to a dilution of the biomarker signal (i.e. dinosterol) within the sediment (Belt, 2018; Lizotte, 2001). Sea-ice concentrations derived from diatom TF show a similar trend within subunit C1 and point towards a reduced WSI cover, even though the WSI concentration still ranges from 65 to 80% (Fig. 3a).

The alleged discrepancy in the reconstructed sea surface conditions, under which subunit C1 was deposited, can be attributed to the different seasons represented by the two sea-ice proxies: While the sea-ice index P_DIPSO_{25} indicates a reduced sea-ice cover during spring and summer, the diatom TF derived WSI concentration reveals reduced but still existing sea-ice cover during the winter months (Fig. 3a). With values between 0.4 and 0.6 wt%, 3 wt% and 40 wt%, respectively, the TOC, $CaCO_3$ and biogenic opal contents in subunit C1 are even higher than in underlying Unit B (Fig. 3). Taking into account that the opal content determined for the sediments of subunit C1 is most likely underestimated because the leaching method applied for its measurement (Hillenbrand et al., 2010) is better suited for quantifying low opal contents (Müller and Schneider, 1993), the productivity proxies indicate high primary productivity, consistent with reduced sea-ice cover during spring and summer inferred from the biomarker data. The magnetic susceptibility values show an absolute minimum of $<10 \times 10^{-5}$ SI units (Fig. 3f), pointing to a very low content of terrigenous components and highlighting the biogenic composition of this subunit. The diatom TF derived WSI data, the biogenic opal and the magnetic susceptibility do, unlike the biomarker record, resolve the lower half of the subunit, suggesting the onset of reduced sea ice during spring and summer at around 12.7 cal. ka BP (239 cmbsf). A similar observation was made by Sjunneskog and Taylor (2002), whose diatom abundance record from Palmer Deep suggests that open water primary productivity commenced at 12.8 ka BP. The grain size distribution shows no significant change, unlike the phase of ice shelf break-up/retreat recorded in Unit B.

Based on these findings we conclude that during deposition of subunit C1 spring and summer sea-ice cover reached its minimum (Fig. 4; Unit C) promoting a higher diatom productivity and the deposition of the diatomaceous ooze. We tentatively suggest that the drastic decrease in spring/summer sea-ice coverage was linked to Antarctic warming that coincided with the onset of the Younger Dryas stadial in the Northern Hemisphere from 12.9-11.7 ka BP (centred at 12.85 ka BP; e.g. Denton et al., 2010). As already noted for the ACR, the environmental conditions at core site PS69/274–1 may have been subject to local oceanic and atmospheric controls rather than to global teleconnections and attempts to relate these observations to interhemispheric feedback mechanisms certainly require more data from the Amundsen Sea and robust chronologies. However, the assignment of this minimum sea-ice/high productivity interval with the Younger Dryas is supported by AIO ^{14}C dates obtained from the diatomaceous ooze in subunit C1 and in other cores recovered offshore from the westernmost Getz Ice Shelf (Hillenbrand et al., 2010, Figs. 2 and 3).

The reliability of these ages is considered high for three reasons: (1) AIO ^{14}C ages obtained from sediments with very high biogenic contents, such as the very pure diatomaceous ooze of subunit C1, provide reliable dates because of high contents of fresh organic matter (e.g., Andrews et al., 1999); (2) the marine setting distal from the ice sheet grounding line implies that it is less affected by contamination with reworked fossil organic matter (Hillenbrand et al., 2010); and (3) confirmation by the RPI age model (Hillenbrand et al., 2010).

In subunit C2 from 196 to 150 cmbsf, concentrations of $IPSO_{25}$ range from 6 to 16 $\mu g^{*}g\ OC^{-1}$ and are significantly higher than in the underlying subunit C1. The phytoplankton-derived biomarker dinosterol also shows significantly higher concentrations of 300–600 $\mu g^{*}g\ OC^{-1}$, relative to the underlying subunit. The calculated sea-ice index P_DIPSO_{25} values around 0.7 resemble those in Unit B, which was deposited during the post-LGM break-up/retreat of the Getz Ice Shelf (Fig. 2a). Rising $IPSO_{25}$ concentrations

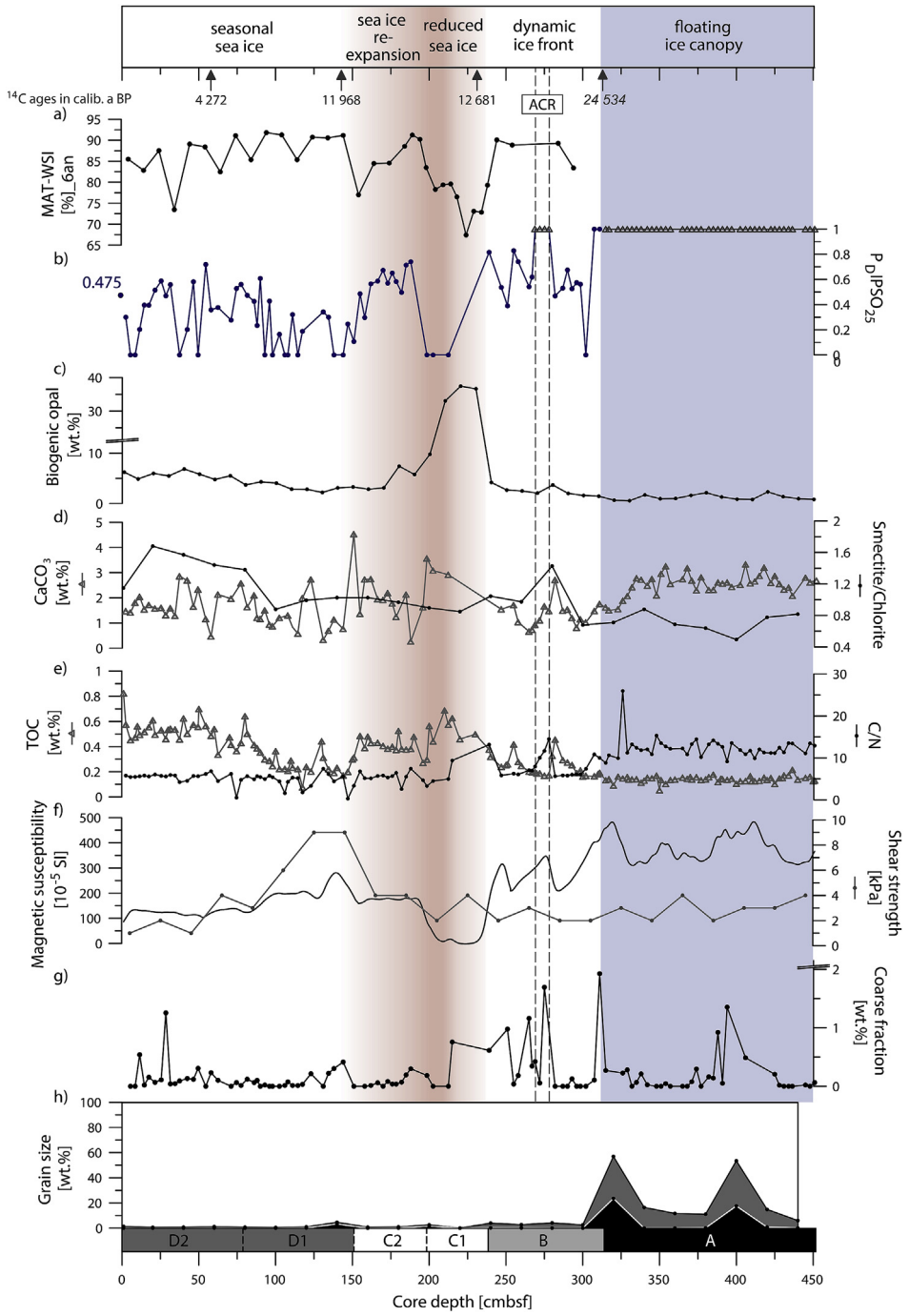

Fig. 3. Winter sea-ice concentrations based on diatom transfer functions (a), P_DIPSO_{25} (b), biogenic opal (c), $CaCO_3$ and smectite/chlorite ratio (d), TOC and C/N ratio (e), magnetic susceptibility and shear strength (f), content of coarse-grained terrigenous debris (>0.5 mm; determined on distinct biomarker samples prior grinding; g) and contents of mud (0–63 μm; white infill), sand (63 μm-2 mm; grey infill) and gravel (>2 mm; black infill; h) for sediment core PS69/274-1. AMS ^{14}C age constraints in calib. a BP in dark grey; unreliable age given in italics (Hillenbrand et al., 2010). Interval highlighted by dashed grey line marks the Antarctic Cold Reversal (ACR; Jouzel et al., 1995). Calculated P_DIPSO_{25} value of the surface sample (multi-core PS69/275-2) indicated by blue dot with black circle and label in respective color. Triangles in P_DIPSO_{25}-curve: thick ice cover, maximum value of 1 assigned to these samples. Core is divided into four units as indicated in the lowermost and topmost bar: Unit A: floating ice canopy (blue shading), Unit B: dynamic ice front, Unit C: reduced sea ice/sea-ice re-expansion (red shading), Unit D: seasonal sea ice, as indicated in Fig. 2. (For interpretation of the references to color in this figure legend, the reader is referred to the Web version of this article.)

point to a re-expansion of spring sea-ice cover, while the strong increase and high concentrations in dinosterol point to either ice-free summer sea surface conditions or sustained ice-edge phytoplankton blooms. Primary production in marginal ice zones (MIZ) can exceed that of the permanently open ocean (Belt, 2018; Lizotte, 2001) and would explain the maximum concentration of dinosterol in subunit C2. Since diatom derived TF reconstructions for this subunit indicate a WSI concentration of 90%, we assume that sea ice prevailed also during spring (promoting $IPSO_{25}$ synthesis) but retreated in summer (permitting phytoplankton growth). TOC concentrations vary around an average value of 0.4 wt%, whilst magnetic susceptibility values are also relatively constant (mean

value of 150× 10^{-5} SI units; Fig. 3e and f). Likewise, there is no significant change in grain sizes in comparison to that of subunit C1, with mainly silt and clay being deposited (Fig. 3h).

Based on these findings we conclude that subunit C2 reflects a time of sea-ice re-expansion during spring, which allowed for a high production of $IPSO_{25}$. We suggest that this interval of sea-ice re-expansion coincided with the end of the Younger Dryas stadial in the Northern Hemisphere, which is roughly consistent with the AIO ^{14}C date of 11 989 cal. a BP (Hillenbrand et al., 2010, Figs. 2 and 3).

4.1.4. Unit D: Seasonal sea-ice cover environment

The uppermost Unit D (150-0 cmbsf) spans the time after ca 12 ka BP (Hillenbrand et al., 2010) and is marked by highly variable biomarker concentrations. It can be divided into two subunits (D1 and D2).

In subunit D1 (150-80 cmbsf) concentrations of the sea-ice biomarker $IPSO_{25}$ are characterised by low values of ca 1 μg*g OC^{-1} (Fig. 2c), while concentrations of the phytoplankton-derived biomarker dinosterol are more variable (100–400 μg*g OC^{-1}; Fig. 2b). The generally low P_DIPSO_{25} values of 0–0.4 suggest a reduced sea-ice cover during deposition of subunit D1 (Fig. 2a). In contrast, the diatom derived TF reconstructions indicate maximum WSI concentrations of ca 92% (Fig. 3a). These contrasting reconstructions highlight the potential limitations of the P_DIPSO_{25} proxy, which are discussed in more detail in section 5. At 140 cmbsf core depth, a minimum observed in both biomarker proxies coincides with a TOC minimum and elevated magnetic susceptibility values and gravel content (Fig. 3). The high values in magnetic susceptibility are in this case likely due to less dilution from biogenic material rather than increased terrigenous flux associated with IRD input or advance of the grounding line. Shear strength data in core PS69/274-1 show a significant increase from 3 to 9 kPa in subunit D1 (Fig. 3f), which is also observed in other cores offshore from the westernmost Getz Ice Shelf (Hillenbrand et al., 2010; Smith et al., 2011) and possibly results from the slightly coarse-grained composition of this sediment interval as it is evident from the elevated gravel contents.

The upper subunit D2 (80-0 cmbsf) shows highly variable concentrations of the sea-ice biomarker $IPSO_{25}$ ranging between 0 and 12 μg*g OC^{-1} (Fig. 2c), while intermediate concentrations of the phytoplankton-derived biomarker dinosterol vary from 200 to 500 μg*g OC^{-1} (Fig. 2b). The sea-ice index P_DIPSO_{25} fluctuates between 0 and 0.7 (Fig. 2a), indicating highly variable sea-ice conditions. Diatom-based TF reveals WSI concentrations between 73 and 90% (Fig. 3a). TOC contents reach highest concentrations in the record (0.8 wt%; Fig. 3e), indicating relatively high productivity during this time interval, which is also supported by the increase in biogenic opal concentration throughout subunit D2 with values from 2 to 7 wt% (Fig. 3c). Magnetic susceptibility values slightly decrease upwards throughout the subunit from ca 200 to 120 × 10^{-5} SI units, while the grain size remains unchanged with almost 100% mud content (Fig. 3f and h). The decreasing magnetic susceptibility values may refer to a reduced input of siliciclastic material resulting in lower sedimentation rates, which in turn may have led to a relative enrichment in biogenic material.

Concentrations of the coarse grains >0.5 mm are relatively constant throughout Unit D, with a few distinct peaks up to 1.2 wt% in subunit D2 (Fig. 3g; 26 cmbsf, 12.5 cmbsf). Based on these findings, we assume that Unit D in core PS69/274-1 was deposited in a seasonally open marine (i.e. only sea-ice covered during winter and spring) setting similar to today, while the overall co-occurrence and the in-phase changes of both biomarkers are potentially attributable to the establishment of the ASP (Fig. 4; Unit D) favouring both $IPSO_{25}$ producing sea-ice diatom productivity as well as ice-edge phytoplankton blooms (cf. Belt, 2018). In this regard, we refer to Campagne et al. (2015) who reveal that each calving event of the Mertz Glacier Tongue (East Antarctica) since the last 250 years results in elevated abundances of $IPSO_{25}$ followed by a slow decrease of the sea-ice proxy and a concomitant increase of open-water proxies. Campagne et al. (2015) and Nihashi and Ohshima (2015) both conclude that local, rather than regional/global dynamics, such as the calving and regrowth of glacier tongues or landfast sea ice, play an important role in the formation

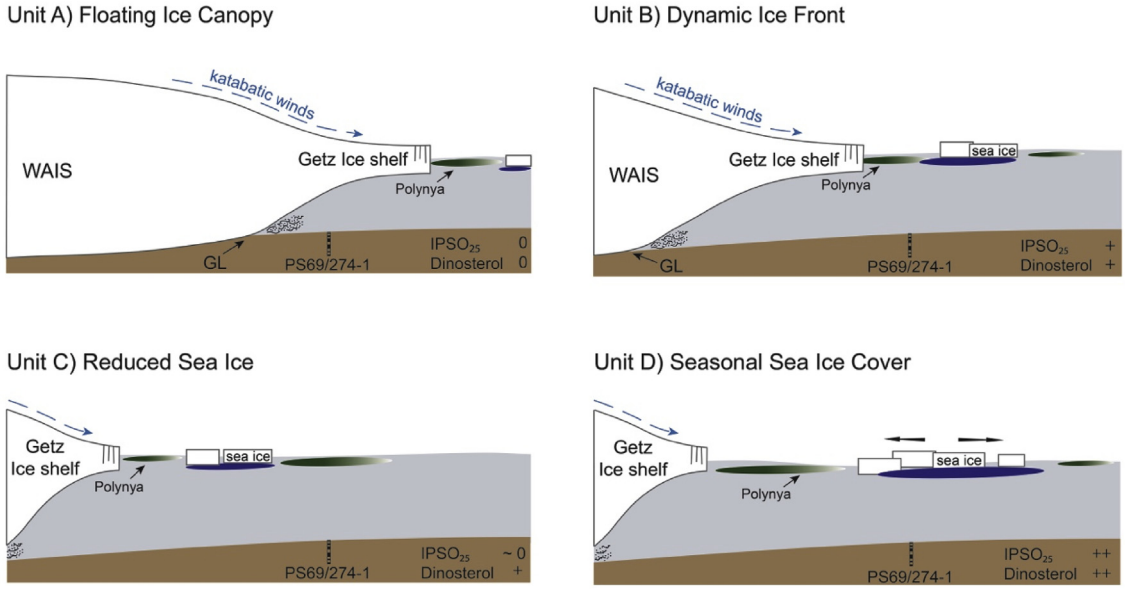

Fig. 4. Schematic cross-section showing the core location of sediment core PS69/274-1, illustrating the four general phases (Unit A-D) of sea-ice cover evolution and the retreat of the Getz Ice Shelf. Note that reconstruction refers to spring/summer sea-ice conditions. Production areas of $IPSO_{25}$ are shown in blue, phytoplankton dinosterol in green and input of coarse-grained debris >0.5 mm at grounding line (GL); WAIS: West Antarctic Ice Sheet. (For interpretation of the references to color in this figure legend, the reader is referred to the Web version of this article.)

and variability of polynya conditions and the resulting sedimentary biomarker/proxy records. Constraining polynya dynamics, however, is very challenging, since it is still debated, for example, whether the high productivity within the ASP is really archived in the underlying sediments (Kim et al., 2016) or not (Lee et al., 2017). Hence, it is important to make this subject a focus of future research. The limited availability of Holocene age constraints for core PS69/274-1 impedes direct comparisons with other marine records, from e.g. the Antarctic Peninsula, documenting warming and cooling periods such as the Mid Holocene Climatic Optimum or the Neoglacial (e.g. Heroy et al., 2008; Milliken et al., 2009; Sjunneskog and Taylor, 2002). However, we note that also the overall trends in $IPSO_{25}$, dinosterol and TOC in Unit D do not exhibit significant similarity with records from the Antarctic Peninsula and hence tentatively suggest that the environment at the core site was controlled by local, potentially ASP, conditions.

5. Applicability of the combined open-water phytoplankton biomarker and $IPSO_{25}$ approach

The $PIPSO_{25}$ approach combines information on ocean surface conditions derived from sea-ice algae and open-water phytoplankton. In this respect, it has the potential to be a powerful semi-quantitative tool for reconstructing sea-ice cover during the past. However, it is apparent that this novel proxy also has its limitations that need to be considered in order to establish robust interpretations. Most open-water phytoplankton biomarkers have multiple source organisms and are not specific to certain environments. Although dinoflagellates are the major source of the herein used open-water phytoplankton dinosterol, it is not unique to these organisms and is also found in diatoms (Volkman et al., 1993; Volkman, 2006). Despite the different sources of dinosterol, it can still be considered a useful proxy for open water environments, since it has not yet been found in any other organisms of sympagic origin (Belt et al., 2018). Furthermore, selective degradation of $IPSO_{25}$ and phytoplankton biomarkers likely influences the ratio between their source and sedimentary environments (Rontani et al., 2019a, b). More in-situ studies investigating the transport and preservation of HBIs and sterols under varying oceanographic conditions (including different sedimentation rates) are needed to address these aspects.

Despite the need for further investigations to overcome these specific knowledge gaps, the combined approach of $PIPSO_{25}$ can help circumvent misleading interpretations, such as over-/underestimations of sea-ice cover on the basis of high/low $IPSO_{25}$ concentrations in the sediments. It is, however, important to carefully interpret the $PIPSO_{25}$ index when, for instance, fluctuations of $IPSO_{25}$ and the phytoplankton biomarker are in-phase. On the basis of work in the Arctic, Müller et al. (2011) demonstrated that coevally high (for marginal ice zone conditions) or low (for a perennial sea-ice cover) concentrations of both biomarkers can lead to similar PIP_{25} values, despite the very different sea-ice conditions. The same principle also applies to the $PIPSO_{25}$ index, suggesting the need to interpret these data alongside other proxies.

Unit D1 (150-80 cmbsf) in core PS69/274-1, for instance, is characterised by intervals of very low concentrations of both biomarkers, which usually reflects unfavourable environmental conditions for sea ice diatoms as well as for phytoplankton. In general, these unfavourable environmental conditions are related to a very thick, perennial (sea) ice cover limiting light availability required for photosynthesis. The calculated low P_DIPSO_{25} values for this interval, however, point to a reduced sea-ice cover. This severe underestimation of sea-ice cover is revealed by the contrasting very high WSI concentrations (up to 90%) derived from diatom TF. This scenario of a more extensive sea-ice cover than inferred from the P_DIPSO_{25} index is additionally supported by relatively low TOC concentrations and high magnetic susceptibility values. It is therefore important to carefully interpret the $PIPSO_{25}$ index not only in combination with other biomarker records but also alongside other proxy records, such as diatom TF data and sedimentological parameters.

6. Summary and conclusions

Changes in ice shelf/sea-ice cover in the western ASE since the post-LGM deglaciation have been reconstructed using the sea-ice proxy $IPSO_{25}$ and the phytoplankton-derived biomarker dinosterol. For a semi-quantitative reconstruction of ice cover, the phytoplankton-$IPSO_{25}$ index (P_DIPSO_{25}) was applied and compared to both WSI concentrations derived from diatom TF reconstructions and environmental constraints deduced from sedimentological data.

The Getz Ice Shelf and sea-ice cover in the study area show a dynamic behaviour since the last deglaciation with a first break-up or retreat of the ice shelf and the establishment of a dynamic ice front just before 13 cal. ka BP. During the break-up/retreat phase, the biomarker proxy records tentatively suggest either a brief re-advance of the ice shelf or the temporary establishment of a perennial sea-ice cover, which could be linked to atmospheric cooling during the Antarctic Cold Reversal. Following this episode, the biomarker records reveal a phase with significantly reduced sea-ice cover during spring and summer around 12.7 cal. ka BP, which was characterised by deposition of a relatively pure diatomaceous ooze. This phase may be linked to a warming in Antarctica, which potentially coincided with the onset of the Younger Dryas stadial in the Northern Hemisphere, and may thus document interhemispheric climate coupling via the bipolar seesaw. After the predominantly open marine phase, a re-expansion of spring sea ice occurred in the western ASE and was followed by highly variable sea-ice conditions throughout the Holocene.

Our study demonstrates that pairing $IPSO_{25}$ and a phytoplankton biomarker has the potential to provide a valuable proxy for the assessment of past sea-ice environments in Antarctica. However, to obtain robust palaeoenvironmental information, we recommend that the biomarker lipids are applied alongside other proxies, including diatom TF and TOC data and sedimentological parameters.

Data availability

Datasets related to this article can be found online on *PANGAEA Data Publisher for Earth & Environmental Science* (doi:10.1594/PANGAEA.904263).

Declaration of competing interest

None.

Acknowledgements

Denise Diekstall, Maximilian Mues, Robert Grosser and Mandy Kuck are kindly acknowledged for laboratory support. We thank the captain, crew and science party of RV *Polarstern* cruise PS69. Simon Belt is acknowledged for providing the 7-HND internal standard for HBI quantification. N.L. and J.M were funded through the Helmholtz Research Grant VH-NG-1101. J.A.S and C.D.H were funded by NERC grant NE/M013081/1. G.K. was funded through the research program PACES II: Polar Regions and Coasts in the changing EarthSystem.

Appendix A. Supplementary data

Supplementary data to this article can be found online at https://doi.org/10.1016/j.quascirev.2019.106103.

References

Alderkamp, A.-C., Mills, M.M., van Dijken, G.L., Laan, P., Thuróczy, C.-E., Gerringa, L.J., de Baar, H.J., Payne, C.D., Visser, R.J., Buma, A.G., 2012. Iron from melting glaciers fuels phytoplankton blooms in the Amundsen Sea (Southern Ocean): phytoplankton characteristics and productivity. Deep Sea Res. Part II Top. Stud. Oceanogr. 71, 32–48.

Allen, C.S., Pike, J., Pudsey, C.J., 2011. Last glacial–interglacial sea-ice cover in the SW Atlantic and its potential role in global deglaciation. Quat. Sci. Rev. 30, 2446–2458.

Anderson, R., Ali, S., Bradtmiller, L., Nielsen, S., Fleisher, M., Anderson, B., Burckle, L., 2009. Wind-driven upwelling in the Southern Ocean and the deglacial rise in atmospheric CO2. Science 323, 1443–1448.

Andrews, J.T., 1987. Late quaternary marine sediment accumulation in fiord-shelf-deep-sea transects, Baffin island to Baffin Bay. Quat. Sci. Rev. 6, 231–243.

Andrews, J.T., Domack, E.W., Cunningham, W.L., Leventer, A., Licht, K.J., Jull, A.T., DeMaster, D.J., Jennings, A.E., 1999. Problems and possible solutions concerning radiocarbon dating of surface marine sediments, Ross Sea, Antarctica. Quat. Res. 52, 206–216.

Armand, L., Zielinski, U., 2001. Diatom species of the genus Rhizosolenia from Southern Ocean sediments: distribution and taxonomic notes. Diatom Res. 16, 259–294.

Armand, L.K., Crosta, X., Romero, O., Pichon, J.-J., 2005. The biogeography of major diatom taxa in Southern Ocean sediments: 1. Sea ice related species. Palaeogeogr. Palaeoclimatol. Palaeoecol. 223, 93–126.

Arndt, J.E., Schenke, H.W., Jakobsson, M., Nitsche, F., Buys, G., Goleby, B., Rebesco, M., Bohoyo, F., Hong, J.K., Black, J., Greku, R., Udintsev, G., Barrios, F., Reynoso-Peralta, W., Morishita, T., Wigley, R., 2013. The International Bathymetric Chart of the Southern Ocean (IBCSO) Version 1.0 - a new bathymetric compilation covering circum-Antarctic waters. Geophys. Res. Lett. 40, 3111–3117. https://doi.org/10.1002/grl.50413.

Arrigo, K.R., Van Dijken, G.L., 2003. Phytoplankton dynamics within 37 Antarctic coastal polynya systems. J. Geophys. Res. 108 (C8), 3271. https://doi.org/10.1029/2002JC001739.

Arrigo, K.R., Lowry, K.E., van Dijken, G.L., 2012. Annual changes in sea ice and phytoplankton in polynyas of the Amundsen Sea, Antarctica. Deep Sea Res. Part II Top. Stud. Oceanogr. 71–76, 5–15.

Arrigo, K.R., van Dijken, G.L., Strong, A.L., 2015. Environmental controls of marine productivity hot spots around Antarctica. J. Geophys. Res.: Oceans 120, 5545–5565.

Barbara, L., Crosta, X., Massé, G., Ther, O., 2010. Deglacial environments in eastern Prydz Bay, East Antarctica. Quat. Sci. Rev. 29, 2731–2740.

Belt, S.T., Allard, W.G., Massé, G., Robert, J.-M., Rowland, S.J., 2000. Highly branched isoprenoids (HBIs): identification of the most common and abundant sedimentary isomers. Geochem. Cosmochim. Acta 64, 3839–3851.

Belt, S.T., Massé, G., Rowland, S.J., Poulin, M., Michel, C., LeBlanc, B., 2007. A novel chemical fossil of palaeo sea ice: IP25. Org. Geochem. 38, 16–27.

Belt, S.T., Müller, J., 2013. The Arctic sea ice biomarker IP25: a review of current understanding, recommendations for future research and applications in palaeo sea ice reconstructions. Quat. Sci. Rev. 79, 9–25.

Belt, S.T., Brown, T.A., Ampel, L., Cabedo-Sanz, P., Fahl, K., Kocis, J.J., Masse, G., Navarro-Rodriguez, A., Ruan, J., Xu, Y., 2014. An inter-laboratory investigation of the Arctic sea ice biomarker proxy IP25 in marine sediments: key outcomes and recommendations. Clim. Past 10, 155–166.

Belt, S.T., Smik, L., Brown, T.A., Kim, J.H., Rowland, S.J., Allen, C.S., Gal, J.K., Shin, K.H., Lee, J.I., Taylor, K.W.R., 2016. Source identification and distribution reveals the potential of the geochemical Antarctic sea ice proxy IPSO25. Nat. Commun. 7, 12655. https://doi.org/10.1038/ncomms12655.

Belt, S.T., Brown, T.A., Smik, L., Assmy, P., Mundy, C., 2018. Sterol identification in floating Arctic sea ice algal aggregates and the Antarctic sea ice diatom *Berkeleya adeliensis*. Org. Geochem. 118, 1–3.

Belt, S.T., 2018. Source-specific biomarkers as proxies for Arctic and Antarctic sea ice. Org. Geochem. 125, 277–298.

Benz, V., Esper, O., Gersonde, R., Lamy, F., Tiedemann, R., 2016. Last Glacial Maximum sea surface temperature and sea-ice extent in the Pacific sector of the Southern Ocean. Quat. Sci. Rev. 146, 216–237.

Berkman, P.A., Forman, S.L., 1996. Pre-bomb radiocarbon and the reservoir correction for calcareous marine species in the Southern Ocean. Geophys. Res. Lett. 23, 363–366.

Bianchi, C., Gersonde, R., 2004. Climate evolution at the last deglaciation: the role of the Southern Ocean. Earth Planet. Sci. Lett. 228, 407–424.

Blunier, T., Schwander, J., Stauffer, B., Stocker, T., Dällenbach, A., Indermühle, A., Tschumi, J., Chappellaz, J., Raynaud, D., Barnola, J.M., 1997. Timing of the Antarctic Cold reversal and the atmospheric CO2 increase with respect to the younger Dryas event. Geophys. Res. Lett. 24, 2683–2686.

Blunier, T., Brook, E.J., 2001. Timing of millennial-scale climate change in Antarctica and Greenland during the last glacial period. Science 291, 109–112.

Boon, J.J., Rijpstra, W.I.C., de Lange, F., De Leeuw, J., Yoshioka, M., Shimizu, Y., 1979. Black Sea sterol—a molecular fossil for dinoflagellate blooms. Nature 277, 125–127.

Bopp, L., Kohfeld, K.E., Le Quéré, C., Aumont, O., 2003. Dust impact on marine biota and atmospheric CO2 during glacial periods. Paleoceanography 18 (2), 1046. https://doi.org/10.1029/2002PA000810.

Broecker, W.S., 1998. Paleocean circulation during the last deglaciation: a bipolar seesaw? Paleoceanography 13, 119–121.

Campagne, P., Crosta, X., Houssais, M.-N., Swingedouw, D., Schmidt, S., Martin, A., Devred, E., Capo, S., Marieu, V., Closset, I., 2015. Glacial ice and atmospheric forcing on the Mertz Glacier Polynya over the past 250 years. Nat. Commun. 6, 6642. https://doi.org/10.1038/ncomms7642.

Collins, L.G., Allen, C.S., Pike, J., Hodgson, D.A., Weckström, K., Massé, G., 2013. Evaluating highly branched isoprenoid (HBI) biomarkers as a novel Antarctic sea-ice proxy in deep ocean glacial age sediments. Quat. Sci. Rev. 79, 87–98.

Comiso, J.C., Gersten, R.A., Stock, L.V., Turner, J., Perez, G.J., Cho, K., 2017. Positive Trend in the Antarctic sea ice cover and associated changes in surface temperature. J. Clim. 30, 2251–2267.

Crosta, X., Pichon, J.J., Burckle, L., 1998. Application of modern analog technique to marine Antarctic diatoms: reconstruction of maximum sea-ice extent at the Last Glacial Maximum. Paleoceanography Paleoclimatol. 13, 284–297.

Crosta, X., Romero, O., Armand, L.K., Pichon, J.-J., 2005. The biogeography of major diatom taxa in Southern Ocean sediments: 2. Open ocean related species. Palaeogeogr. Palaeoclimatol. Palaeoecol. 223, 66–92.

Cuffey, K.M., Clow, G.D., Steig, E.J., Buizert, C., Fudge, T., Koutnik, M., Waddington, E.D., Alley, R.B., Severinghaus, J.P., 2016. Deglacial temperature history of West Antarctica. Proc. Natl. Acad. Sci. 113, 14249–14254.

Denis, D., Crosta, X., Barbara, L., Massé, G., Renssen, H., Ther, O., Giraudeau, J., 2010. Sea ice and wind variability during the Holocene in East Antarctica: insight on middle–high latitude coupling. Quat. Sci. Rev. 29, 3709–3719.

Denton, G.H., Anderson, R.F., Toggweiler, J., Edwards, R., Schaefer, J., Putnam, A., 2010. The last glacial termination. Science 328, 1652–1656.

De Santis, A., Maier, E., Gomez, R., Gonzalez, I., 2017. Antarctica, 1979–2016 sea ice extent: total versus regional trends, anomalies, and correlation with climatological variables. Int. J. Remote Sens. 38, 7566–7584.

Domack, E., 1992. Modern carbon-14 ages and reservoir corrections for the Antarctic Peninsula and Gerlache Strait area. Antarct. J. U. S. 27, 63–64.

Domack, E.W., Mcclennen, C.E., 1996. Accumulation of glacial marine sediments in fjords of the Antarctic Peninsula and their use as late Holocene paleoenvironmental indicators. Found. Ecol. Res. West Antarct. Peninsula 70, 135–154.

Ehrmann, W., Hillenbrand, C.-D., Smith, J.A., Graham, A.G., Kuhn, G., Larter, R.D., 2011. Provenance changes between recent and glacial-time sediments in the Amundsen Sea embayment, West Antarctica: clay mineral assemblage evidence. Antarct. Sci. 23, 471–486.

Esper, O., Gersonde, R., Kadagies, N., 2010. Diatom distribution in southeastern Pacific surface sediments and their relationship to modern environmental variables. Palaeogeogr. Palaeoclimatol. Palaeoecol. 287, 1–27.

Esper, O., Gersonde, R., 2014a. New tools for the reconstruction of Pleistocene Antarctic sea ice. Palaeogeogr. Palaeoclimatol. Palaeoecol. 399, 260–283.

Esper, O., Gersonde, R., 2014b. Quaternary surface water temperature estimations: new diatom transfer functions for the Southern Ocean. Palaeogeogr. Palaeoclimatol. Palaeoecol. 414, 1–19.

Etourneau, J., Collins, L.G., Willmott, V., Kim, J.-H., Barbara, L., Leventer, A., Schouten, S., Damsté, J.S., Bianchini, A., Klein, V., 2013. Holocene climate variations in the western Antarctic Peninsula: evidence for sea ice extent predominantly controlled by changes in insolation and ENSO variability. Clim. Past 9, 1431–1446.

Fahl, K., Stein, R., 2012. Modern seasonal variability and deglacial/Holocene change of central Arctic Ocean sea-ice cover: new insights from biomarker proxy records. Earth Planet. Sci. Lett. 351, 123–133.

Fetterer, F., Knowles, K., Meier, W., Savoie, M., Windnagel, A.K., 2016. Updated Daily. Sea Ice Index, Version 2. [Median Sea Ice Extent 1981-2010]. NSIDC: National Snow and Ice Data Center, Boulder, Colorado USA. https://doi.org/10.7265/N5736NV7 [24 July 2017].

Gersonde, R., Zielinski, U., 2000. The reconstruction of late Quaternary Antarctic sea-ice distribution—the use of diatoms as a proxy for sea-ice. Palaeogeogr. Palaeoclimatol. Palaeoecol. 162, 263–286.

Gersonde, R., Crosta, X., Abelmann, A., Armand, L., 2005. Sea-surface temperature and sea ice distribution of the Southern Ocean at the EPILOG Last Glacial Maximum—a circum-Antarctic view based on siliceous microfossil records. Quat. Sci. Rev. 24, 869–896.

Gohl, K., 2007. The expedition ANTARKTIS-XXIII/4 of the research vessel Polarstern in 2006. In: Berichte zur Polar-und Meeresforschung (Reports on Polar and Marine Research), Bremerhaven, Alfred Wegener Institute for Polar and Marine Research, vol. 557, p. 166. https://doi.org/10.2312/BzPM_0557_2007.

Graham, A.G.C., Kuhn, G., Meisel, O., Hillenbrand, C.-D., Hodgson, D.A., Ehrmann, W., Wacker, L., Wintersteller, P., dos Santos Ferreira, C., Römer, M., White, D., Bohrmann, G., 2017. Major advance of South Georgia glaciers during the Antarctic Cold Reversal following extensive sub-Antarctic glaciation. Nat. Commun. 8, 14798. https://doi.org/10.1038/ncomms14798.

Hall, A., 2004. The role of surface albedo feedback in climate. J. Clim. 17, 1550–1568.

Hasle, G.R., Syvertsen, E.E., 1996. Marine diatoms. In: Tomas, C.R. (Ed.), Identifying Marine Diatoms and Dinoflagellates. Academic Press Limited, London, pp. 5–385.

Hellmer, H.H., Kauker, F., Timmermann, R., Determann, J., Rae, J., 2012. Twenty-first-century warming of a large Antarctic ice-shelf cavity by a redirected coastal

current. Nature 485, 225–228.
Heroy, D.C., Anderson, J.B., 2007. Radiocarbon constraints on Antarctic Peninsula ice sheet retreat following the last glacial maximum (LGM). Quat. Sci. Rev. 26, 3286–3297.
Heroy, D.C., Sjunneskog, C., Anderson, J.B., 2008. Holocene climate change in the Bransfield Basin, Antarctic Peninsula: evidence from sediment and diatom analysis. Antarct. Sci. 20, 69–87.
Hillenbrand, C.D., Smith, J.A., Kuhn, G., Esper, O., Gersonde, R., Larter, R.D., Maher, B., Moreton, S.G., Shimmield, T.M., Korte, M., 2010. Age assignment of a diatomaceous ooze deposited in the western Amundsen sea embayment after the last glacial maximum. J. Quat. Sci. 25, 280–295.
Hillenbrand, C.-D., Kuhn, G., Smith, J.A., Gohl, K., Graham, A.G., Larter, R.D., Klages, J.P., Downey, R., Moreton, S.G., Forwick, M., 2013. Grounding-line retreat of the west Antarctic ice sheet from inner Pine island Bay. Geology 41, 35–38.
Hillenbrand, C.-D., Smith, J.A., Hodell, D.A., Greaves, M., Poole, C.R., Kender, S., Williams, M., Andersen, T.J., Jernas, P.E., Elderfield, H., Klages, J.P., Roberts, S.J., Gohl, K., Larter, R.D., Kuhn, G., 2017. West Antarctic Ice Sheet retreat driven by Holocene warm water incursions. Nature 547, 43–48.
Hutson, W.H., 1980. The Agulhas current during the late pleistocene: analysis of modern faunal analogs. Science 207, 64–66.
Jacobs, S.S., Jenkins, A., Giulivi, C.F., Dutrieux, P., 2011. Stronger ocean circulation and increased melting under Pine Island Glacier ice shelf. Nat. Geosci. 4, 519–523.
Jenkins, A., Dutrieux, P., Jacobs, S.S., McPhail, S.D., Perrett, J.R., Webb, A.T., White, D., 2010. Observations beneath pine island glacier in west Antarctica and implications for its retreat. Nat. Geosci. 3, 468–472.
Jenkins, A., Shoosmith, D., Dutrieux, P., Jacobs, S., Kim, T.W., Lee, S.H., Ha, H.K., Stammerjohn, S., 2018. West Antarctic ice sheet retreat in the Amundsen sea driven by decadal oceanic variability. Nat. Geosci. 11, 733–738.
Jouzel, J., Vaikmae, R., Petit, J., Martin, M., Duclos, Y., Stievenard, M., Lorius, C., Toots, M., Mélières, M., Burckle, L., 1995. The two-step shape and timing of the last deglaciation in Antarctica. Clim. Dyn. 11, 151–161.
Kern, S., 2009. Wintertime Antarctic coastal polynya area: 1992–2008. Geophys. Res. Lett. 36, L14501. https://doi.org/10.1029/2009GL038062.
Kim, M., Hwang, J., Kim, H.J., Kim, D., Yang, E.J., Ducklow, H.W., La Hyoung, S., Lee, S.H., Park, J., Lee, S., 2015. Sinking particle flux in the sea ice zone of the Amundsen shelf, Antarctica. Deep Sea Res. Oceanogr. Res. Pap. 101, 110–117.
Kim, M., Hwang, J., Lee, S.H., Kim, H.J., Kim, D., Yang, E.J., Lee, S., 2016. Sedimentation of particulate organic carbon on the Amundsen Shelf, Antarctica. Deep Sea Res. Part II Top. Stud. Oceanogr. 123, 135–144.
Lee, S., Hwang, J., Ducklow, H.W., Hahm, D., Lee, S.H., Kim, D., Hyun, J.H., Park, J., Ha, H.K., Kim, T.W., 2017. Evidence of minimal carbon sequestration in the productive Amundsen Sea polynya. Geophys. Res. Lett. 44, 7892–7899.
Leventer, A., Domack, E.W., Ishman, S.E., Brachfeld, S., McClennen, C.E., Manley, P., 1996. Productivity cycles of 200–300 years in the Antarctic Peninsula region: understanding linkages among the sun, atmosphere, oceans, sea ice, and biota. Geol. Soc. Am. Bull. 108, 1626–1644.
Leventer, A., 1998. The fate of Antarctic “sea ice diatoms” and their use as paleoenvironmental indicators. Antarct. Sea Ice. Biol. Process., Interact. Var. 121–137.
Lizotte, M.P., 2001. The contributions of sea ice algae to Antarctic marine primary production. Am. Zool. 41, 57–73.
Maddison, E.J., Pike, J., Leventer, A., Domack, E.W., 2005. Deglacial seasonal and subseasonal diatom record from Palmer Deep, Antarctica. J. Quat. Sci.: Pub. Quat. Res. Assoc. 20, 435–446.
Maqueda, M.M., Willmott, A.J., Biggs, N.R.T., 2004. Polynya dynamics: a review of observations and modeling. Rev. Geophys. 42, RG1004. https://doi.org/10.1029/2002RG000116.
Martin, S., 2001. Polynyas. In: Steele, J.H. (Ed.), Encyclopedia of Ocean Sciences, second ed. Academic Press, Oxford, pp. 540–545.
Massé, G., Belt, S.T., Crosta, X., Schmidt, S., Snape, I., Thomas, D.N., Rowland, S.J., 2011. Highly branched isoprenoids as proxies for variable sea ice conditions in the Southern Ocean. Antarct. Sci. 23, 487–498.
Massom, R.A., Eicken, H., Hass, C., Jeffries, M.O., Drinkwater, M.R., Sturm, M., Worby, A.P., Wu, X., Lytle, V.I., Ushio, S., 2001. Snow on Antarctic sea ice. Rev. Geophys. 39, 413–445.
Massom, R.A., Scambos, T.A., Bennetts, L.G., Reid, P., Squire, V.A., Stammerjohn, S.E., 2018. Antarctic ice shelf disintegration triggered by sea ice loss and ocean swell. Nature 558, 383–389.
Mathiot, P., Goosse, H., Fichefet, T., Barnier, B., Gallée, H., 2011. Modelling the seasonal variability of the Antarctic Slope current. Ocean Sci. 7, 455–470.
Meredith, M.P., Woodworth, P.L., Chereskin, T.K., Marshall, D.P., Allison, L.C., Bigg, G.R., Donohue, K., Heywood, K.J., Hughes, C.W., Hibbert, A., 2011. Sustained monitoring of the Southern Ocean at Drake passage: past achievements and future priorities. Rev. Geophys. 49, RG4005. https://doi.org/10.1029/2010rg000348.
Milliken, K., Anderson, J., Wellner, J., Bohaty, S., Manley, P., 2009. High-resolution Holocene climate record from Maxwell Bay, South Shetland islands, Antarctica. GSA Bull. 121, 1711–1725.
Minzoni, R.T., Majewski, W., Anderson, J.B., Yokoyama, Y., Fernandez, R., Jakobsson, M., 2017. Oceanographic influences on the stability of the Cosgrove ice shelf, Antarctica. Holocene 27, 1645–1658.
Müller, P.J., Schneider, R., 1993. An automated leaching method for the determination of opal in sediments and particulate matter. Deep Sea Res. Oceanogr. Res. Pap. 40, 425–444.
Müller, J., Massé, G., Stein, R., Belt, S.T., 2009. Variability of sea-ice conditions in the Fram Strait over the past 30,000 years. Nat. Geosci. 2, 772–776.
Müller, J., Wagner, A., Fahl, K., Stein, R., Prange, M., Lohmann, G., 2011. Towards quantitative sea ice reconstructions in the northern North Atlantic: a combined biomarker and numerical modelling approach. Earth Planet. Sci. Lett. 306, 137–148.
Nakayama, Y., Schröder, M., Hellmer, H.H., 2013. From circumpolar deep water to the glacial meltwater plume on the eastern Amundsen Shelf. Deep Sea Res. Oceanogr. Res. Pap. 77, 50–62.
Nicholls, K.W., Østerhus, S., Makinson, K., Gammelsrød, T., Fahrbach, E., 2009. Ice-ocean processes over the continental shelf of the southern Weddell Sea, Antarctica: a review. Rev. Geophys. 47, RG3003. https://doi.org/10.1029/2007RG000250.
Nihashi, S., Ohshima, K.I., 2015. Circumpolar mapping of Antarctic coastal polynyas and landfast sea ice: relationship and variability. J. Clim. 28, 3650–3670.
Orsi, A.H., Whitworth III, T., Nowlin Jr., W.D., 1995. On the meridional extent and fronts of the Antarctic Circumpolar Current. Deep Sea Res. Oceanogr. Res. Pap. 42, 641–673.
Parkinson, C.L., Cavalieri, D.J., 2012. Antarctic sea ice variability and trends, 1979–2010. Cryosphere 6, 871–880. https://doi.org/10.5194/tc-6-871-2012.
Parkinson, C.L., 2019. A 40-y record reveals gradual Antarctic sea ice increases followed by decreases at rates far exceeding the rates seen in the Arctic. Proc. Natl. Acad. Sci. 116, 14414–14423.
Pedro, J.B., Van Ommen, T., Rasmussen, S., Morgan, V.I., Chappellaz, J., Moy, A.D., Masson-Delmotte, V., Delmotte, M., 2011. The last deglaciation: timing the bipolar seesaw. Clim. Past 7, 671–683.
Pedro, J.B., Bostock, H.C., Bitz, C.M., He, F., Vandergoes, M.J., Steig, E.J., Chase, B.M., Krause, C.E., Rasmussen, S.O., Markle, B.R., 2016. The spatial extent and dynamics of the Antarctic Cold Reversal. Nat. Geosci. 9, 51–55.
Perrette, M., Yool, A., Quartly, G.D., Popova, E.E., 2011. Near-ubiquity of ice-edge blooms in the Arctic. Biogeosciences 8, 515–524.
Reynolds, R.W., Rayner, N.A., Smith, T.M., Stokes, D.C., Wang, W., 2002. An improved in situ and satellite SST analysis for climate. J. Clim. 15, 1609–1625.
Reynolds, R.W., Smith, T.M., Liu, C., Chelton, D.B., Casey, K.S., Schlax, M.G., 2007. Daily high-resolution-blended analyses for sea surface temperature. J. Clim. 20, 5473–5496.
Riaux-Gobin, C., Poulin, M., 2004. Possible symbiosis of Berkeleya adeliensis Medlin, Synedropsis fragilis (Manguin) Hasle et al. and Nitzschia lecointei Van Heurck (Bacillariophyta) associated with land-fast ice in Adélie Land, Antarctica. Diatom Res. 19, 265–274.
Romero, O.E., Armand, L.K., Crosta, X., Pichon, J.J., 2005. The biogeography of major diatom taxa in Southern Ocean surface sediments: 3. Tropical/Subtropical species. Palaeogeogr. Palaeoclimatol. Palaeoecol. 223, 49–65.
Rontani, J.-F., Smik, L., Belt, S.T., Vaultier, F., Armbrecht, L., Leventer, A., Armand, L.K., 2019a. Abiotic degradation of highly branched isoprenoid alkenes and other lipids in the water column off East Antarctica. Mar. Chem. 210, 34–47.
Rontani, J.-F., Smik, L., Belt, S.T., 2019b. Autoxidation of the sea ice biomarker proxy IPSO25 in the near-surface oxic layers of Arctic and Antarctic sediments. Org. Geochem. 129, 63–76.
Rosenblum, E., Eisenman, I., 2017. Sea ice trends in climate models only accurate in runs with biased global warming. J. Clim. 30, 6265–6278.
Schrader, H., Gersonde, R., 1978. Diatoms and silicoflagellates. In: Zachariasse, W.J., Riedel, W.R., Sanfilippo, A., Schmidt, R.R., Brolsma, M.J., Schrader, H.J., Gersonde, R., Drooger, M.M., Broekman, J.A. (Eds.), Micropaleontological Methods and Techniques - an Exercise on an Eight Meter Section of the Lower Pliocene of Capo Rossello, Sicily, vol. 17. Utrecht Micropaleontol. Bull, pp. 129–176.
Shepherd, A., Wingham, D., Rignot, E., 2004. Warm ocean is eroding West Antarctic ice sheet. Geophys. Res. Lett. 31, L23402. https://doi.org/10.1029/2004GL021284.
Shepherd, A., Fricker, H.A., Farrell, S.L., 2018. Trends and connections across the Antarctic cryosphere. Nature 558, 223–232.
Sjunneskog, C., Taylor, F., 2002. Postglacial marine diatom record of the Palmer deep, Antarctic Peninsula (ODP Leg 178, Site 1098) 1. Total diatom abundance. Paleoceanography 17 (PAL 4–1-PAL), 4–8.
Skinner, L.C., Fallon, S., Waelbroeck, C., Michel, E., Barker, S., 2010. Ventilation of the deep Southern Ocean and deglacial CO_2 rise. Science 328, 1147–1151.
Smik, L., Cabedo-Sanz, P., Belt, S.T., 2016. Semi-quantitative estimates of paleo Arctic sea ice concentration based on source-specific highly branched isoprenoid alkenes: a further development of the PIP_{25} index. Org. Geochem. 92, 63–69.
Smith, W.O., Nelson, D.M., 1986. Importance of ice edge phytoplankton production in the Southern Ocean. Bioscience 36, 251–257.
Smith Jr., W.O., 1987. Phytoplankton dynamics in marginal ice zones. Oceanogr. Mar. Biol. 25, 11–38.
Smith, J.A., Hillenbrand, C.-D., Kuhn, G., Larter, R.D., Graham, A.G., Ehrmann, W., Moreton, S.G., Forwick, M., 2011. Deglacial history of the west Antarctic ice sheet in the western Amundsen sea embayment. Quat. Sci. Rev. 30, 488–505.
Stammerjohn, S., Massom, R., Rind, D., Martinson, D., 2012. Regions of rapid sea ice change: an inter-hemispheric seasonal comparison. Geophys. Res. Lett. 39, L06501. https://doi.org/10.1029/2012GL050874.
Stammerjohn, S., Maksym, T., Massom, R., Lowry, K., Arrigo, K., Yuan, X., Raphael, M., Randall-Goodwin, E., Sherrell, R., Yager, P., 2015. Seasonal sea ice changes in the Amundsen Sea, Antarctica, over the period of 1979–2014. Elem Sci. Anth 3. https://doi.org/10.12952/journal.elementa.000055.
Thoma, M., Jenkins, A., Holland, D., Jacobs, S., 2008. Modelling circumpolar deep water intrusions on the Amundsen Sea continental shelf, Antarctica. Geophys. Res. Lett. 35, L18602. https://doi.org/10.1029/2008GL034939.

Thomas, D.N., 2017. Sea Ice. John Wiley & Sons.
Vaughan, D.G., Comiso, J.C., Allison, I., Carrasco, J., Kaser, G., Kwok, R., Mote, P., Murray, T., Paul, F., Ren, J., 2013. Observations: cryosphere. Clim. Change 2103, 317–382.
Volkman, J.K., 1986. A review of sterol markers for marine and terrigenous organic matter. Org. Geochem. 9, 83–99.
Volkman, J.K., Barrett, S.M., Dunstan, G.A., Jeffrey, S.W., 1993. Geochemical significance of the occurrence of dinosterol and other 4-methyl sterols in a marine diatom. Org. Geochem. 20, 7–15.
Volkman, J.K., 2006. Lipid markers for marine organic matter. In: Marine Organic Matter: Biomarkers, Isotopes and DNA. Springer, pp. 27–70.
Vorrath, M.-E., Müller, J., Esper, O., Mollenhauer, G., Haas, C., Schefuß, E., Fahl, K., 2019. Highly branched isoprenoids for Southern Ocean sea ice reconstructions: a pilot study from the Western Antarctic Peninsula. Biogeosciences 16, 2961–2981.
WAIS Divide Project Members, 2013. Onset of deglacial warming in West Antarctica driven by local orbital forcing. Nature 500, 440–444.
Xiao, W., Esper, O., Gersonde, R., 2016. Last glacial-holocene climate variability in the Atlantic sector of the Southern Ocean. Quat. Sci. Rev. 135, 115–137.
Xiao, X., Fahl, K., Müller, J., Stein, R., 2015. Sea-ice distribution in the modern Arctic Ocean: biomarker records from trans-Arctic Ocean surface sediments. Geochem. Cosmochim. Acta 155, 16–29.
Yager, P.L., Sherrell, R.M., Stammerjohn, S.E., Alderkamp, A.-C., Schofield, O., Abrahamsen, E.P., Arrigo, K.R., Bertilsson, S., Garay, D.L., Guerrero, R., 2012. ASPIRE: the Amundsen Sea Polynya international research expedition. Oceanography 25, 40–53.
Zielinski, U., Gersonde, R., 1997. Diatom distribution in Southern Ocean surface sediments (Atlantic sector): implications for paleoenvironmental reconstructions. Palaeogeogr. Palaeoclimatol. Palaeoecol. 129, 213–250.
Zielinski, U., Gersonde, R., Sieger, R., Fütterer, D., 1998. Quaternary surface water temperature estimations: calibration of a diatom transfer function for the Southern Ocean. Paleoceanography Paleoclimatol. 13, 365–383.

Update

Quaternary Science Reviews
Volume 234, Issue , 15 April 2020, Page

DOI: https://doi.org/10.1016/j.quascirev.2020.106260

Quaternary Science Reviews 234 (2020) 106260

Contents lists available at ScienceDirect

Quaternary Science Reviews

journal homepage: www.elsevier.com/locate/quascirev

Corrigendum

Corrigendum to "Highly branched isoprenoids reveal onset of deglaciation followed by dynamic sea-ice conditions in the western Amundsen Sea, Antarctica" [Quat. Sci. Rev. 228 (2020) 106103]

Nele Lamping [a, *], Juliane Müller [a, b, c], Oliver Esper [a], Claus-Dieter Hillenbrand [d], James A. Smith [d], Gerhard Kuhn [a]

[a] Alfred-Wegener-Institut Helmholtz-Zentrum für Polar- und Meeresforschung, Am Alten Hafen 26, 27568, Bremerhaven, Germany
[b] Department of Geosciences, University of Bremen, Klagenfurter Straße, 28359, Bremen, Germany
[c] Marum - Center for Marine Environmental Sciences, Leobener Straße 8, 28359, Bremen, Germany
[d] British Antarctic Survey, High Cross, Madingley Road, Cambridge, CB3 0ET, United Kingdom

After publication of the article, the authors noticed a mistake in the concentration calculations of the two biomarker lipids $IPSO_{25}$ and dinosterol. The volume of the internal standards 7-hexylnonadecane and 5α-androstan-3-ol had incorrectly been calculated twice. Hence, the absolute concentrations of $IPSO_{25}$ are erroneously higher by factor 20 and the concentrations of dinosterol are erroneously higher by factor 60. The calculated P_DIPSO_{25} index is not affected by these changes.

In 4.1.2. Unit B: Dynamic ice front

The value for $IPSO_{25}$ was reported as 4–8 μg*g OC^{-1}, but should now be corrected to 0.2–0.4 μg*g OC^{-1}.
The value for dinosterol was reported as 200–400 μg*g OC^{-1}, but should now be corrected to ca 2–7 μg*g OC^{-1}.

In 4.1.3. Unit C: Reduced sea-ice cover followed by sea-ice re-expansion

In subunit C1, the value for dinosterol was reported as 180 μg*g OC^{-1}, but should be corrected to 3 μg*g OC^{-1}.
In subunit C2, the value for $IPSO_{25}$ was reported as 6–16 μg*g OC^{-1}, but should be corrected to 0.3–0.8 μg*g OC^{-1}.
In subunit C2, the value for dinosterol was reported as 300–600 μg*g OC^{-1}, but should be corrected to 5–10 μg*g OC^{-1}.

In 4.1.4. Unit D: Seasonal sea-ice cover environment

In subunit D1, the value for $IPSO_{25}$ was reported as ca 1 μg*g OC^{-1}, but should be corrected to ca 0.05 μg*g OC^{-1}.
In subunit D1, the value for dinosterol was reported as 100–400 μg*g OC^{-1}, but should be corrected to ca 1–7 μg*g OC^{-1}.
In subunit D2, the value for $IPSO_{25}$ was reported as 0–12 μg*g OC^{-1}, but should be corrected to 0–0.2 μg*g OC^{-1}.
In subunit D2, the value for dinosterol was reported as 200–500 μg*g OC^{-1}, but should be corrected to ca 3–8 μg*g OC^{-1}.

Please note that the values of the $IPSO_{25}$ and dinosterol axes in Fig. 2. and the corresponding supplementary figure plotted versus age (printed below) are now corrected.

Datasets uploaded to PANGAEA Data Publisher for Earth & Environmental Science have also been corrected (https://doi.org/10.1594/PANGAEA.904263).

The changes have no impact on the scientific results and reasoning presented in the paper.

DOI of original article: https://doi.org/10.1016/j.quascirev.2019.106103.
* Corresponding author. Am Alten Hafen 26, 27568, Bremerhaven, Germany.
E-mail addresses: nele.lamping@awi.de (N. Lamping), juliane.mueller@awi.de (J. Müller), oliver.esper@awi.de (O. Esper), hilc@bas.ac.uk (C.-D. Hillenbrand), jaas@bas.ac.uk (J.A. Smith), gerhard.kuhn@awi.de (G. Kuhn).

https://doi.org/10.1016/j.quascirev.2020.106260
0277-3791/

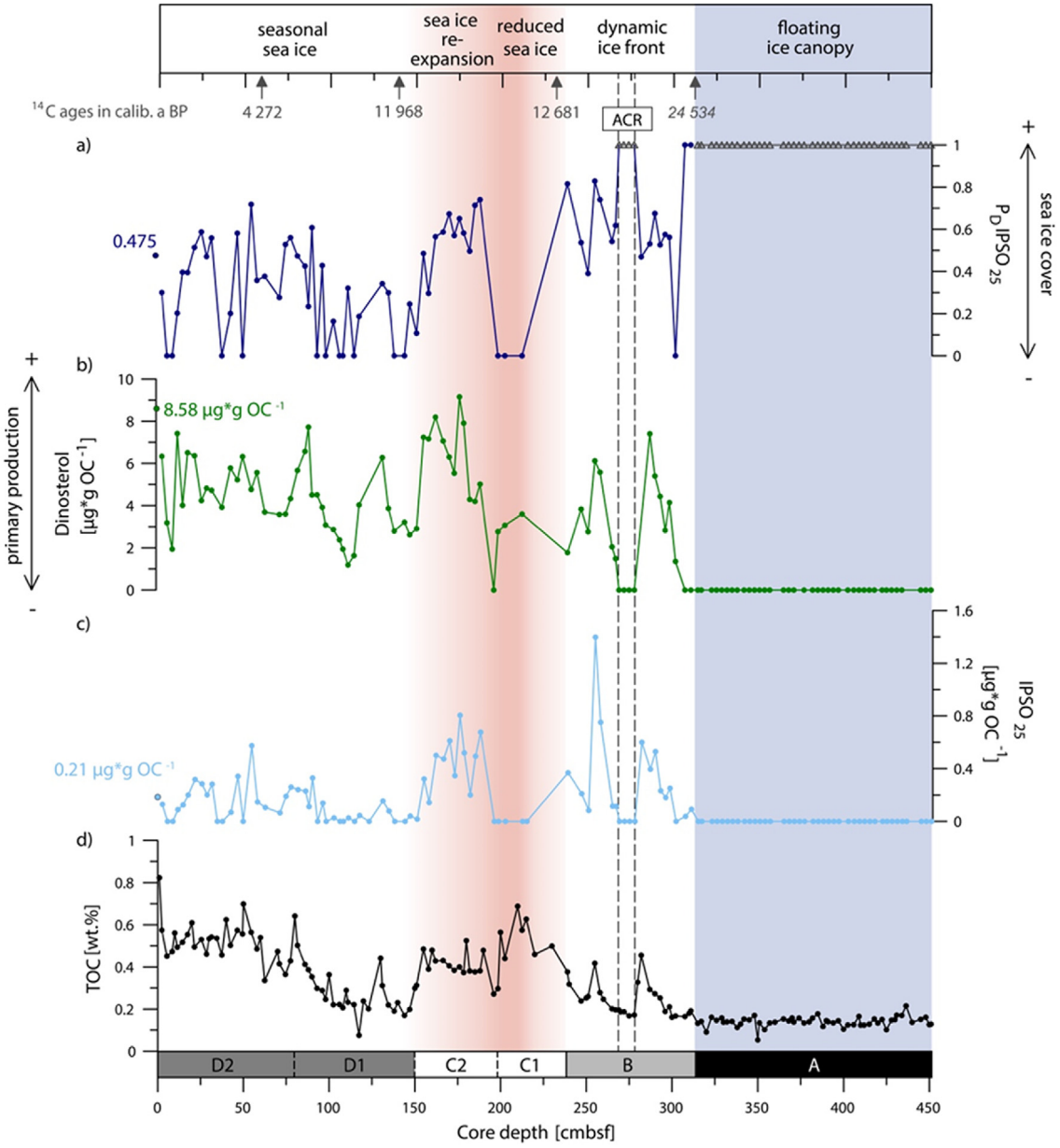

Fig. 2. Contents of P_DIPSO_{25} (a), dinosterol (b), $IPSO_{25}$ (c) and TOC (d) in sediment core PS69/274-1. AMS ^{14}C age constraints in calib. a before present (BP) in dark grey; unreliable age given in italics (Hillenbrand et al., 2010). Interval highlighted by dashed grey line marks the Antarctic Cold Reversal (ACR; Jouzel et al., 1995). Biomarker concentrations and calculated P_DIPSO_{25} value of the surface sample (box core PS69/275-2) indicated by dots with black circle and label in respective color. Triangles in P_DIPSO_{25}-curve: thick ice cover, maximum value of 1 assigned to these samples. Core is divided into four units as indicated in the lowermost and topmost bar: Unit A: floating ice canopy (blue shading), Unit B: dynamic ice front, Unit C: reduced sea ice/sea-ice re-expansion (red shading), Unit D: seasonal sea ice. (For interpretation of the references to color in this figure legend, the reader is referred to the Web version of this article.)

Appendix A. Supplementary data

Supplementary data to this article can be found online at https://doi.org/10.1016/j.quascirev.2019.106103.